2. EXPLANATORY NOTES[1]

Shipboard Scientific Party[2]

INTRODUCTION

In this chapter, we have assembled information that will help the reader to understand the observations on which our preliminary conclusions have been based and also help the interested investigator to select samples for further analysis. This information concerns only shipboard operations and analyses described in the site reports in the *Initial Reports* volume of the Leg 149 *Proceedings of the Ocean Drilling Program.* Methods used by various investigators for shore-based analyses of Leg 149 data will be described in the individual scientific contributions to be published in the *Scientific Results* volume.

Authorship of Site Chapters

The separate sections of the site chapters were written by the following shipboard scientists (authors are listed in alphabetical order, no seniority is implied):

Site Summary: Sawyer, Whitmarsh
Background and Objectives: Sawyer, Whitmarsh
Operations: Pollard, Klaus
Site Geophysics: Sawyer, Whitmarsh
Lithostratigraphy: Comas, Marsaglia, Milkert, Milliken, Ramirez, Wilson
Biostratigraphy: Collins, Gervais, de Kaenel, Liu
Paleomagnetism: Kanamatsu, Zhao
Igneous and Metamorphic Petrology and Geochemistry: Beslier, Cornen, Gibson, Seifert
Structural Geology: Beslier, Morgan
Organic Geochemistry: Meyers
Inorganic Geochemistry: Shaw
Physical Properties: Harry, Krawczyk, Morgan, Pinheiro
Downhole Measurements: Hobart, Lofts, Yin
Integration of Seismic Profiles with Observations from the Site: Whitmarsh
Downhole Temperature Measurements: Harry, Hobart, Sawyer
Summary and Conclusions: Sawyer, Whitmarsh

Following the text of all the site chapters, summary core descriptions ("barrel sheets") and photographs of each core are presented in a section called "Cores."

Drilling Characteristics

Core handling and shipboard scientific procedures, including the numbering of sites, holes, cores, sections, and samples were similar to those reported in previous *Initial Reports* volumes of the *Proceedings of the Ocean Drilling Program* (Shipboard Scientific Party, 1993c). Procedures for handling of igneous rock are similar to those used for Leg 147 (Shipboard Scientific Party, 1993a).

At the end of the leg, the cores were transferred from the ship in refrigerated airfreight containers to cold storage at the East Coast Repository of the Ocean Drilling Program, at the Lamont-Doherty Earth Observatory, Columbia University, New York.

LITHOSTRATIGRAPHY

The first part of this section summarizes the methods used to describe sediment cores and the manner in which data collected manually for visual core description forms (VCDs) are summarized and condensed into computer-generated summaries for each core. The second part reviews the sedimentological classifications and terms used in the descriptions.

Visual Core Descriptions (VCDs) of Sedimentary Units

Core Description Forms

Shipboard sedimentologists were responsible for visual core logging, smear-slide analyses, and thin-section descriptions of sedimentary and volcaniclastic material. During Leg 149, information recorded section-by-section on VCD sheets was condensed onto computer-generated summaries that give graphic and textual summaries for each core (see "Cores" section, this volume).

Cores were designated using leg number, site number, hole letter, core number, and core type, as discussed in Shipboard Scientific Party (1993c). The cored interval was specified in terms of meters below sea level (mbsl) and meters below seafloor (mbsf). On the basis of drill-pipe measurements (dpm), reported by the SEDCO Coring Technician and the ODP Operations Superintendent, depths were corrected for the height of the rigfloor dual elevator stool above sea level to give true water depth and correct depth below sea level.

"Graphic Lithology" Column

The lithology of the recovered material is represented on the computer-generated core description forms by symbols representing as many as three components in the column titled "Graphic Lithology" (see bottom right of Fig. 1). Constituents accounting for < 10% of the sediment in a given lithology (or others remaining after the representation of the three most abundant lithologies) are not shown in the "Graphic Lithology" column, but are listed in the "Lithologic Description" section of the core description form. Because of the limitations of the software used for generating the core summaries, the "Graphic Lithology" column shows only the composition of layers or intervals exceeding 20 cm in thickness. This meant that the VCDs for Leg 149 often do not show the nature of vertical changes in the cores, as many of the repetitive sequences present are less than 20 cm thick.

"Age" Column

The chronostratigraphic unit, as recognized on the basis of paleontological and paleomagnetic criteria, is shown in the "Age" col-

[1]Sawyer, D.S., Whitmarsh, R.B., Klaus, A., et al., 1994. *Proc. ODP, Init. Repts.,* 149: College Station, TX (Ocean Drilling Program).
[2]Shipboard Scientific Party is as given in list of participants preceding the contents.

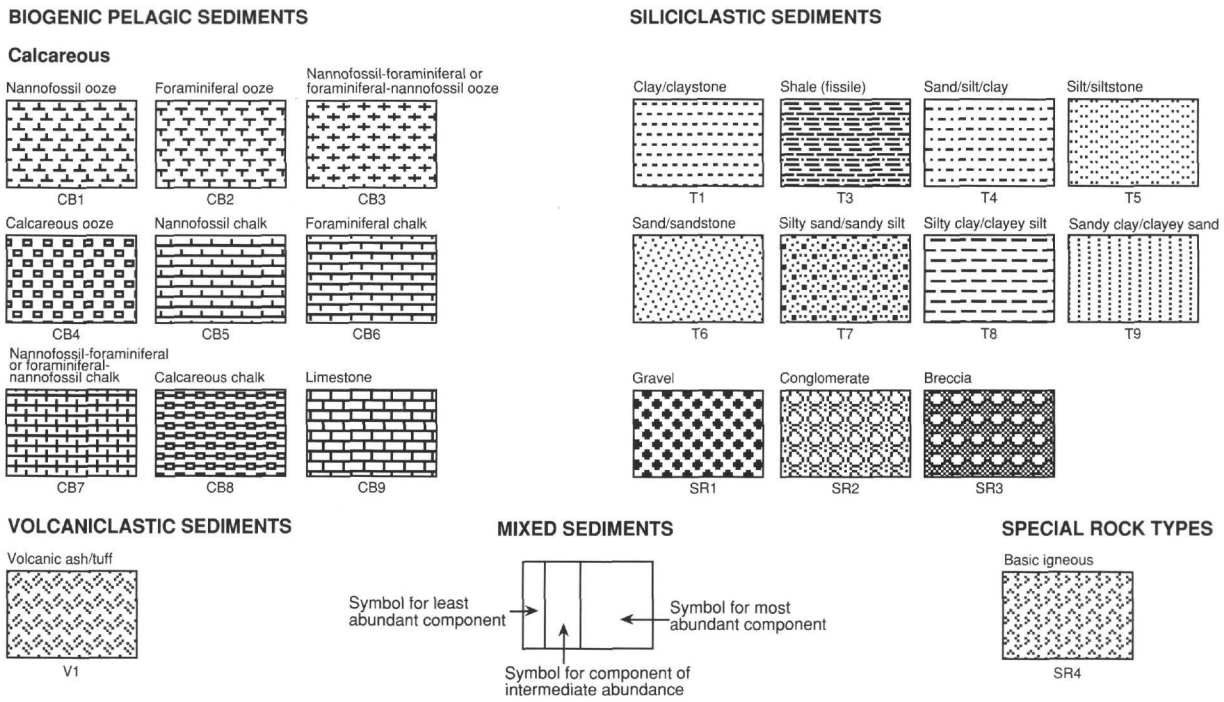

Figure 1. Key to symbols used in the "Graphic Lithology" column on the computer-generated core summaries located in the "Cores" section, this volume.

umn on the core summaries. Boundaries between assigned ages are indicated as follows:

1. *Sharp boundary:* straight line;
2. *Unconformity or hiatus:* line with + signs above it; and
3. *Uncertain:* line with question marks.

"Structure" Column

Natural structures, such as cross stratification, grading, and bioturbation, are indicated in the "Structure" column of the core summaries.

The core summary software also enables color banding to be indicated, but does not include symbols to enable one to record bed thickness. During Leg 149, the shipboard sedimentologists decided to use the color banding symbols to indicate both color banding and interbedded lithologies, as the latter were invariably accompanied by color changes. The following definitions were adopted (from Blatt, Middleton, and Murray, 1980, p. 128):

Thick bedding/color banding	>30 cm
Medium bedding/color banding	10-30 cm
Thin bedding/color banding	<10cm

The core summary software enables sharp and gradational boundaries between color banding to be depicted. Banding showing one sharp boundary and one gradational boundary was arbitrarily defined as having gradational boundaries.

"Disturbance" Column

Sediment disturbance resulting from the coring process may be difficult to distinguish from natural structures. Nonetheless, it is important to estimate the degree and nature of core disturbance in the "Disturbance" column on the core summaries (using symbols in Fig. 2). Blank regions indicate an absence of drilling disturbance. The degree of core disturbance is described for soft and firm sediments using the following categories:

1. *Slightly deformed:* bedding contacts are slightly bent.
2. *Moderately deformed:* bedding contacts are extremely bowed.
3. *Highly deformed:* bedding is completely disturbed, in some places showing symmetrical diapirlike or flow structures.
4. *Soupy:* intervals are water-saturated and have lost all aspects of original bedding.

The degree of fracturing in indurated sediments and igneous rocks is described using the following categories:

1. *Slightly fractured:* core pieces are in place and contain little drilling slurry or breccia;
2. *Moderately fragmented:* core pieces are in place or partly displaced, but the original orientation is preserved or recognizable (drilling slurry may surround fragments);
3. *Lightly fragmented:* pieces are from the cored interval and probably in the correct stratigraphic sequence (although they may not represent the entire section), but the original orientation is completely lost;
4. *Drilling breccia:* core pieces have lost their original orientation and stratigraphic position and may be mixed with drilling slurry.

"Color" Column

The hue and chroma attributes of color were determined using Munsell Soil Color Charts (1971) and recorded in the "Color" column on the core description form.

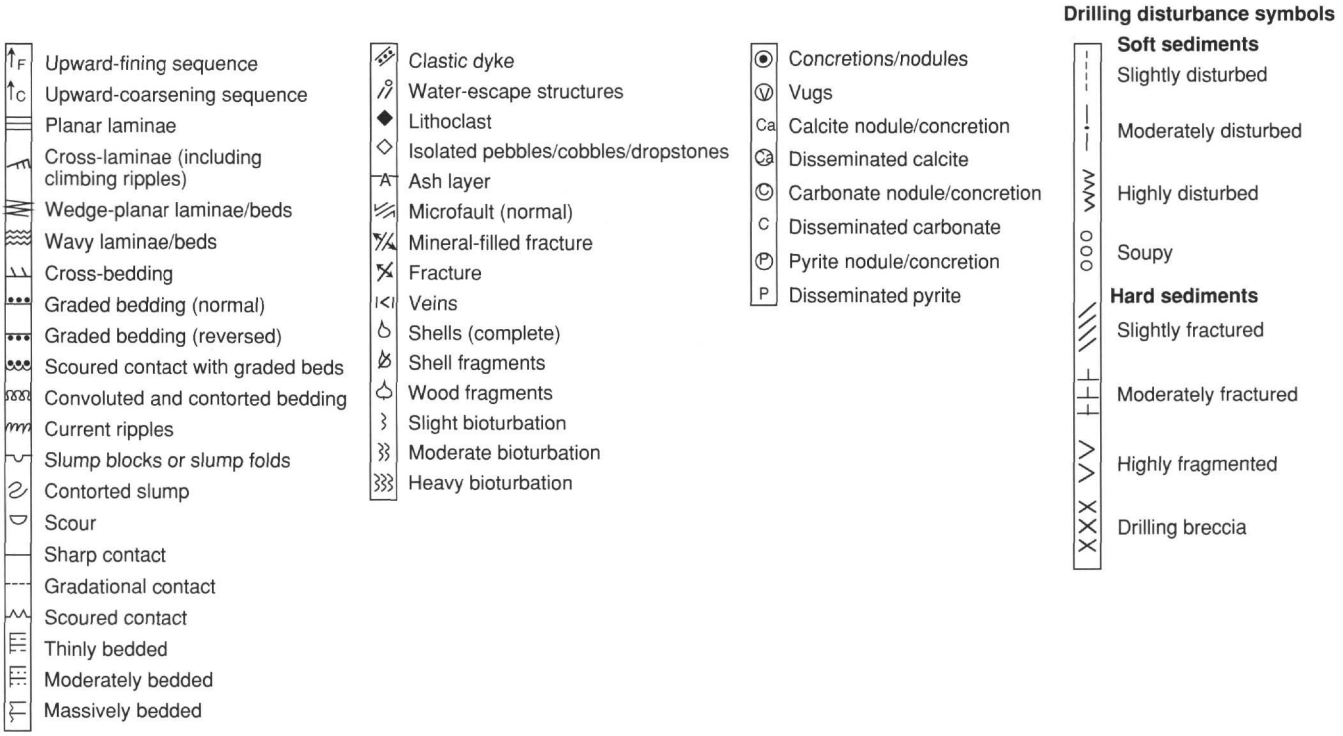

Figure 2. Symbols used for drilling disturbance and sedimentary structures and components on the computer-generated core summaries shown in "Cores" section (this volume).

"Samples" Column

The positions and types of samples taken from each core for shipboard analysis are indicated in the "Samples" column on the core description form, as follows:

C: organic-geochemistry sample,
D: XRD sample,
F: XRF sample,
I: interstitial-water sample,
M: micropaleontology sample,
P: physical-properties sample,
S: smear slide,
T: thin section,
W: whole-round sample, and
X: paleomagnetic sample.

A table summarizing data from smear slide and thin section descriptions appears at the end of each site chapter. The table includes information about the sample location, whether the sample represents a dominant ("D") or a minor ("M") lithology in the core, and the estimated percentages of sand-, silt-, and clay-size material, together with all identified components.

Some samples for carbonate analysis were taken at the same positions from which smear-slide material was taken; additional samples for carbonate analysis were taken by the shipboard geochemists, but the positions of these are not shown on the summaries.

"Description" Column

The lithologic description that appears on each core description form consists of three parts: (1) a heading that lists all the major sedimentary lithologies observed in the core; (2) a heading for minor lithologies, and (3) a more detailed description of the sediments, including features such as color, composition (determined from the smear slides), sedimentary structures, or other notable characteristics. Descriptions and locations of thin, interbedded, or minor lithologies that cannot be depicted in the graphic lithology column, are included in the text.

"Master" Columns

For each hole, a "Master" column was prepared (see "Cores" section, this volume); this indicates core numbers and recovery, graphically summarizes the lithology, and charts a variety of data vs. subbottom depth (biostratigraphic zones, magnetochrons, chemistry, physical properties, and downhole tool measurements). The "Master" columns supplement the information contained on the core description forms, but at a more condensed vertical scale.

Classification of Sediments and Sedimentary Rocks

Introduction

During Leg 149, sedimentologists used a modified version of the ODP sediment classification scheme (Shipboard Scientific Party, 1990; Mazzullo et al., 1987) for granular sediment types (Fig. 3). Variations in the relative proportions of siliciclastic, volcaniclastic, pelagic, and neritic components define five major classes of granular sediments (Fig. 3). The neritic component consists of skeletal and nonskeletal shallow-water bioclasts, including shallow-water benthic foraminifers. Pelagic grains are the skeletal remains of open-marine siliceous and calcareous microfauna and microflora (e.g., radiolarians, diatoms, planktonic foraminifers, nannofossils) and associated organisms. Note that the term micrite is used to define very fine-grained calcareous particles (~<10 µm), observed in smear slides with no clear identification of origin. Calcium carbonate content was qualitatively estimated using smear slides and quantitatively estimated by using coulometric analyses (see "Organic Geochemistry" section, this chapter). Siliciclastic grains are mineral and rock fragments

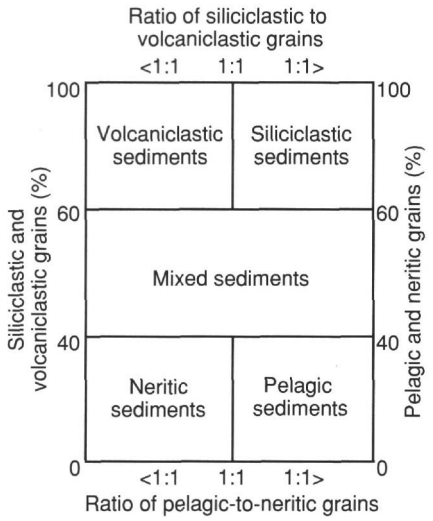

Figure 3. Diagram showing classes of granular sediment (modified from Mazzullo et al., 1987).

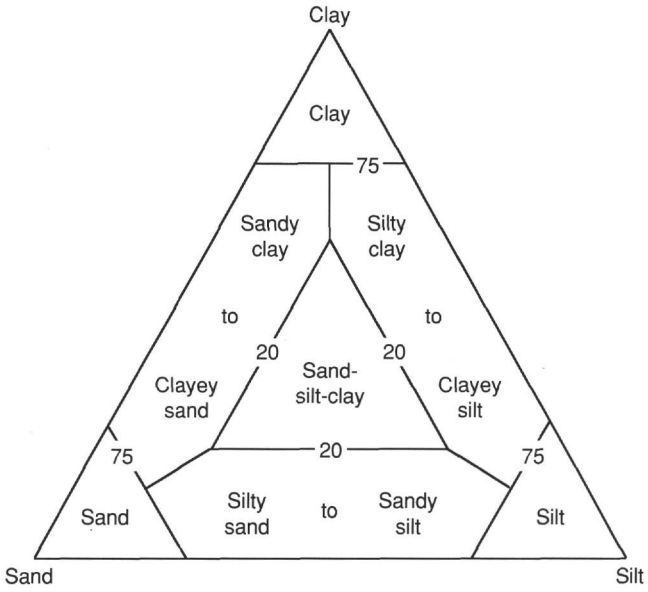

Figure 4. Ternary diagram showing principal names for siliciclastic sediments (modified from Shepard, 1954).

derived from igneous, sedimentary, and metamorphic rocks. Volcaniclastic grains include those of pyroclastic (direct products of magma degassing) and epiclastic (detritus derived from erosion of volcanic rocks) origins.

Granular Sediments

A granular sediment is classified by designating a principal name and major and minor modifiers. The principal name of a granular sediment (e.g., ooze, fine sand or sandstone, volcanic breccia) defines its granular-sediment class as depicted in Figure 3; the major and minor modifiers may include a description of the texture, composition, and fabric.

Siliciclastic Sediments

For siliciclastic sediments, the principal name describes the texture and is assigned according to the following guidelines:

1. The Udden-Wentworth grain-size scale (Wentworth, 1922) defines grain-size ranges and names of the textural groups (gravel, sand, silt, and clay) and subgroups (fine sand, coarse silt, etc.) that are used as the principal names of siliciclastic sediments.
2. Principal names are listed in order of increasing abundance when two or more textural groups or subgroups are present in a siliciclastic sediment (Shepard, 1954; Fig. 4). For simplicity, we have grouped intermediate mixtures of the three textural end members, sand, silt, and clay, into four categories as shown in Figure 4.
3. The suffix "stone" is affixed to the principal names sand, silt, and clay when a saw must be used to cut the core.

Conglomerate and breccia are used as principal names of lithified gravels with well-rounded and angular clasts, respectively.

Pelagic Sediments

For pelagic sediments, the principal name describes the composition and degree of lithification using the following terms:

1. *Ooze:* unlithified calcareous and/or siliceous pelagic sediments;
2. *Chalk:* partially lithified pelagic sediment predominantly composed of calcareous pelagic grains;
3. *Limestone:* lithified pelagic sediment predominantly composed of calcareous pelagic grains; and
4. *Radiolarite, diatomite,* and *spiculite:* partially lithified pelagic sediment predominantly composed of siliceous radiolarians, diatoms, and sponge spicules, respectively.
5. *Porcellanite:* a lithified rock with abundant authigenic silica but less hard, lustrous, or brittle than chert (in part, such rocks may represent mixed sedimentary rock);
6. *Chert:* vitreous or lustrous, conchoidally fractured, lithified rock composed predominantly of authigenic silica.

Major and Minor Modifiers

The principal name of a granular-sediment class is preceded by major modifiers and followed by minor modifiers (the latter preceded by "with") that describe the lithology of the granular sediment in greater detail (e.g., a siliciclastic rock composed of 50% clay, 35% quartz-silt, and 15% foraminifers is classified as a silty claystone with foraminifers). Major and minor modifiers, as applied in the above example, are used most commonly to describe composition and textures of grain types present in major (>25%) and minor (10%-25%) proportions. Major and minor modifiers also may be used to describe grain fabric (e.g., matrix-supported) in siliciclastic and volcaniclastic sediment types.

The composition of pelagic grains can be described with the major and minor modifiers diatom(-aceous), radiolarian, spicule(-ar), siliceous, nannofossil, foraminifer(-al), and calcareous. The terms siliceous and calcareous are used generally to describe sediments composed of siliceous or calcareous pelagic grains of mixed origins.

Grain shape, mineralogy, rock fragment types, fabric, degree of induration, and color can be used as major modifiers. Grain shapes are described by the major modifiers rounded, subrounded, subangular, and angular. The character of siliciclastic grains can be described by mineralogy (using modifiers such as quartzose, feldspathic, glauconitic, micaceous, zeolitic, lithic, or calcareous). Modifiers such as volcanic, sed-lithic, meta-lithic, gneissic, and plutonic, which describe the provenance of rock fragments, also can be used in the clas-

sification of sediments (particularly in gravels, conglomerates, and breccias). The fabric of a sediment can be described as well using major modifiers such as grain-supported, matrix-supported, and imbricated. Generally, fabric terms are useful only when describing gravels, conglomerates, and breccias. The degree of lithification is described using the following major modifiers: "unlithified" designates soft sediment that is readily deformable by finger pressure, "partially lithified" designates firm sediment that is incompletely lithified, and "lithified" designates hard, cemented sediment that must be cut with a saw. Finally, sediment color, as determined visually with the Munsell Soil Color Chart (1971), also can be employed as a major modifier.

Mixed sediments are described using major and minor modifiers indicating composition and texture.

X-ray Diffraction Methods for Fine Fractions

The fine fraction of selected samples was analyzed on board the ship using X-ray diffraction techniques. Sediments were put into suspension by ultrasonic disaggregation, and the fine fraction (<1 µm) was separated by centrifuging and then used to prepare air-dried specimens on glass slides. X-ray diffraction patterns of these oriented specimens were produced using the shipboard Philips AD 3420 X-ray diffractometer (CuK alpha emission source). Selected samples were treated with ethyleneglycol and re-analyzed. Other selected samples were heated at 550°C for 1 to 1.5 hr, and then reanalyzed. Peaks were visually inspected and matched to standard reference peaks for various minerals (quartz, feldspar, hornblende, calcite, pyrite, and clay minerals, etc.).

BIOSTRATIGRAPHY

Preliminary age assignments were established using core-catcher samples. Samples from elsewhere in the cores were examined when a more refined age determination was necessary. Two microfossil groups were examined for biostratigraphic purposes: calcareous nannofossils and planktonic foraminifers. Benthic foraminifers were used to estimate paleobathymetry. Sample positions and the abundance, preservation, and age or zone for each fossil group were recorded on barrel sheets for each core.

The time scales used in this work were those of Berggren, Kent, and van Couvering (1985), Berggren et al. (1985), and Harland et al. (1990) for the Neogene; Cretaceous and Paleogene age assignments are from Berggren et al. (1985), Berggren, Kent, and Flynn (1985), Hallam et al. (1985), and Harland et al. (1990) (Figs. 5 to 8). The age estimates of Cenozoic calcareous nannofossil and planktonic biohorizons have been derived primarily from the geomagnetic polarity time scales (GPTS) of Berggren, Kent, and van Couvering (1985), Berggren et al. (1985), Berggren, Kent, and Flynn (1985), and Hallam et al. (1985). In Tables 1 and 2, we summarize the nannofossil and planktonic foraminifer datums, respectively, used for Leg 149.

Calcareous Nannofossils

Mesozoic Zonation

The Mesozoic zonal schemes of Sissingh (1977) and Roth (1978) were used with additional subdivisions to increase biostratigraphic resolution. No Mesozoic nannofossil zonation has been developed that can provide worldwide application. Further refinement of the sequence of observed biostratigraphic events was provided by Perch-Nielsen (1979; 1985) and Bralower and Siesser (1992).

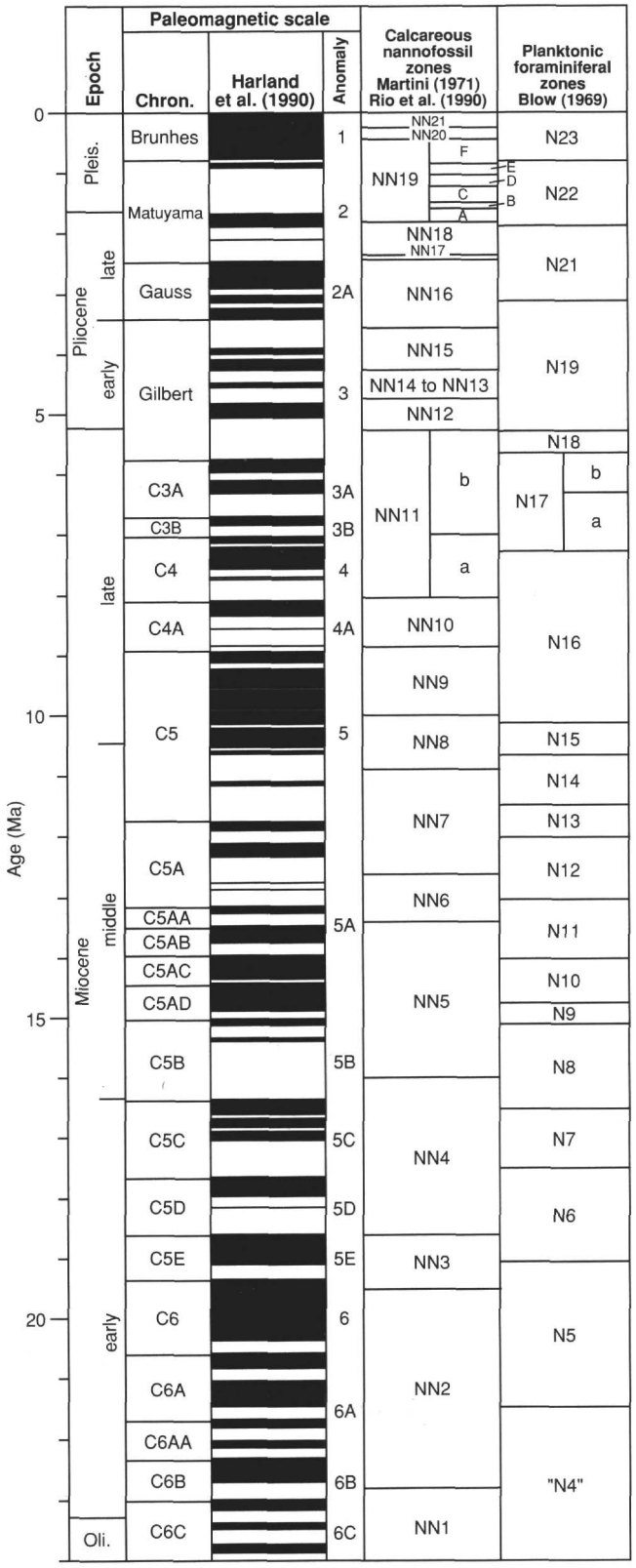

Figure 5. Correlation of the Neogene chronostratigraphy, biostratigraphy, and magnetostratigraphy used during Leg 149. Correlation of the magnetic polarity record and the epoch boundaries follow that of Harland et al. (1990). Data for the calibration of zonal indicators with magnetostratigraphy can be found in Tables 1 and 2.

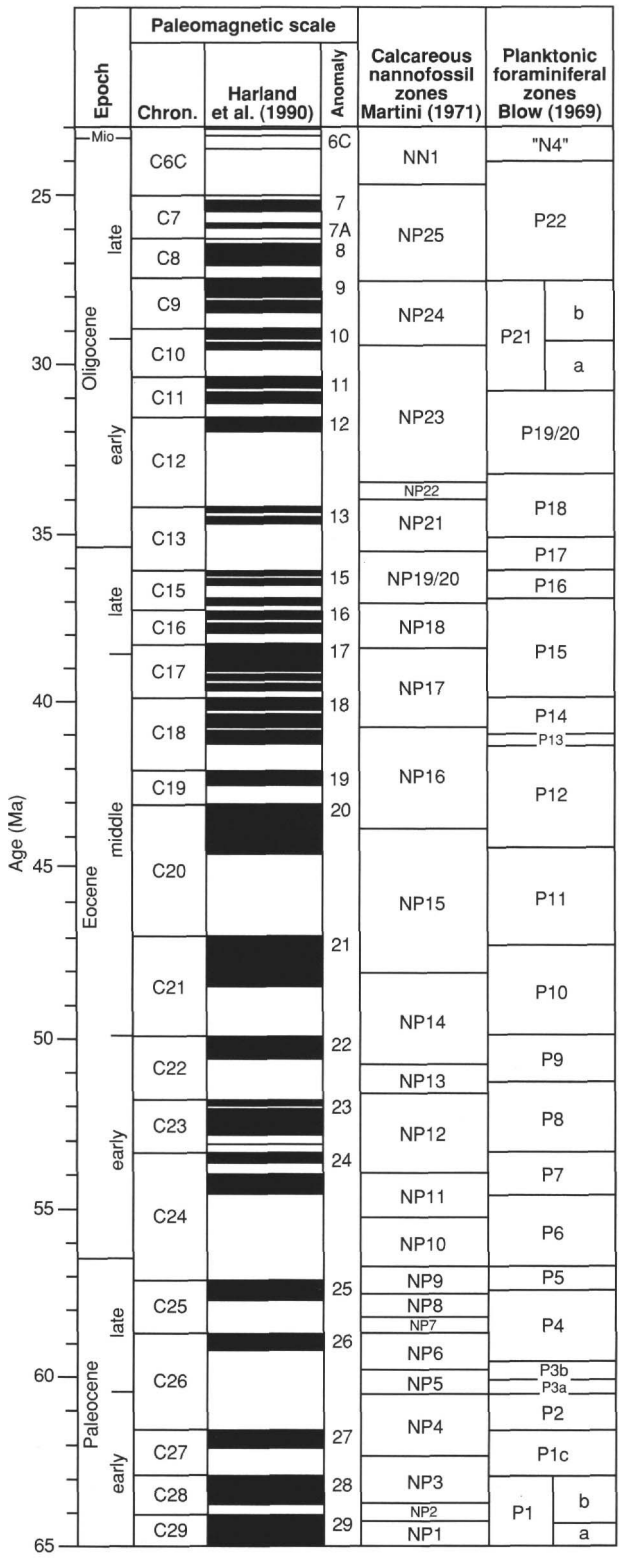

Figure 6. Correlation of the Paleogene chronostratigraphy, biostratigraphy, and magnetostratigraphy used during Leg 149. Correlation of the magnetic polarity record and the epoch boundaries follow that of Harland et al. (1990). Data for the calibration of zonal indicators with magnetostratigraphy can be found in Tables 1 and 2.

Cenozoic Zonation

Ages have been presented in a zonal framework. For convenience, we referred to the zonation and code number of Martini (1971). For Zone NN19, the subzoned scheme from Rio et al. (1990) was used (Subzones NN19A-NN19F). Some important species used by Bukry (1973, 1975), Gartner (1977), and code numbers of Okada and Bukry (1980), as well as newly proposed datum levels, have been incorporated into the Leg 149 stratigraphic framework. Primary and secondary biostratigraphic-event zonal markers for the Cenozoic and Mesozoic are shown in Table 1 and in Figure 8.

Methods

Calcareous nannofossil assemblages were described from smear slides prepared for each core-catcher sample and for as many samples in between as time permitted on board ship. Low-sedimentation-rate (condensed) zones or suspected hiatuses were sampled as closely as was practical. Turbidite sequences were sampled in the hemipelagic and overlying pelagic intervals, and special attention was paid to facies changes. Standard preparation techniques were used throughout. Smear slide examination was done exclusively with a light microscope, using whatever optical configuration yielded useful results. In all cases, a magnification of ×1250 was used to estimate abundance semiquantitatively.

Abundances of individual species were estimated for each sample. Five levels of abundance are recorded, with the following approximate definitions.

R (rare) = 1 specimen per 51-200 fields of view (2-5 specimens total);

F (few) = 1 specimen per 11-50 fields of view (6-15 specimens total);

C (common) = 1 specimen per 2-10 fields of view (16-250 specimens total);

A (abundant) = 1-10 specimens per field of view (251-500 specimens total); and

V (very abundant) = more than 10 specimens per field of view (>500 specimens total).

Estimation of total abundance of calcareous nannofossils for each sample was as follows:

B (barren);

R (rare) = 2-10 specimens for 500 fields of view (about three traverses);

F (few) = 11-50 specimens for 500 fields of view;

C (common) = 51-2000 specimens for 500 fields of view;

A (abundant) = 2,001-20,000 specimens for 500 fields of view; and

V (very abundant) = >20,000 specimens for 500 fields of view.

The qualitative evaluation of the preservation of calcareous nannofossils was recorded as good (G), moderate (M), or poor (P). These categories represent subjective impressions with approximately the following meaning:

P (poor) = Severe dissolution, fragmentation and/or overgrowth has occurred; primary features may have been destroyed and many specimens cannot be identified at the species level;

M (moderate) = Dissolution and/or overgrowth are evident; a significant proportion (up to 25%) of the specimens cannot be identified to species with absolute certainty; and

G (good) = Little or no evidence of dissolution and/or overgrowth is seen; diagnostic characteristics are preserved and nearly all specimens (about 95%) can be identified.

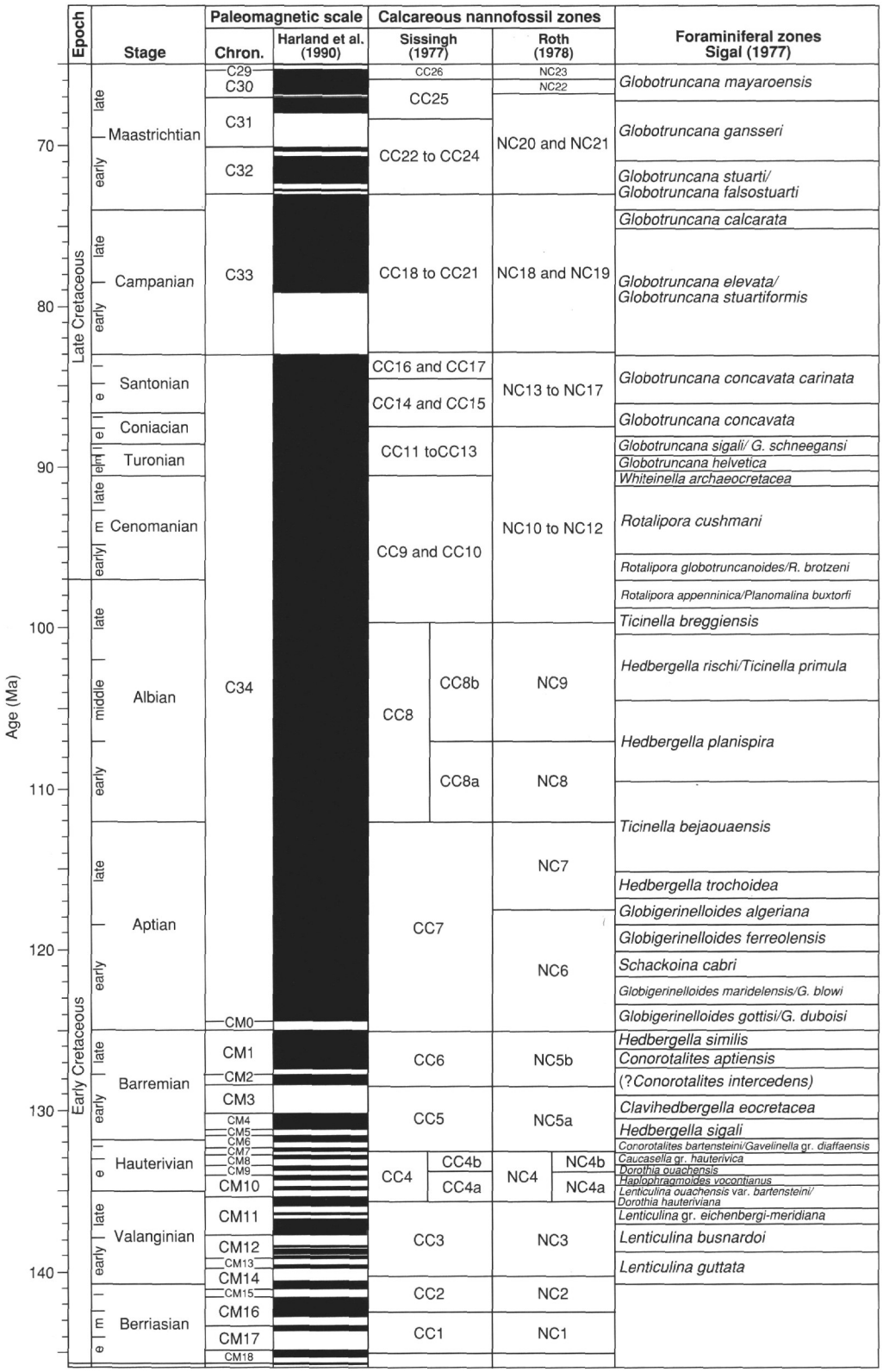

Figure 7. Correlation of the Cretaceous chronostratigraphy, biostratigraphy, and magnetostratigraphy used during Leg 149. Correlation of the magnetic polarity record and the epoch boundaries follow that of Harland et al. (1990).

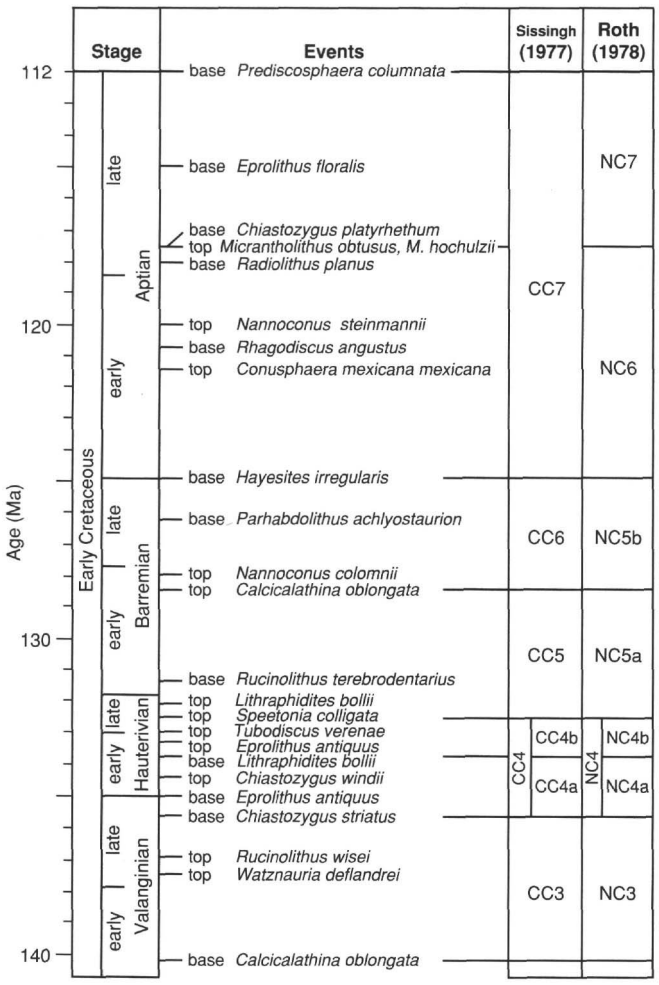

Figure 8. Lower Cretaceous calcareous nannofossil zonation scheme used during Leg 149. Correlation of the magnetic polarity record and stage boundaries follow that of Harland et al. (1990).

Foraminifers

Planktonic Foraminifers

The Cenozoic zonal scheme given by Blow (1969), with slight modifications by Kennett and Srinivasan (1983) and Berggren, Kent, and van Couvering (1985), Berggren et al. (1985) for the Neogene, that of Bolli and Saunders (1985) for the Oligocene to Holocene, and Toumarkine and Luterbacher's (1985) scheme for the Paleocene to Eocene, were employed here. Cretaceous zonations are based on Sigal (1977). Biostratigraphic-event zonal markers for the Cenozoic are shown in Table 2.

Methods

Samples of approximately 10 cm^3 were soaked either in plain tap water or in a Calgon solution and washed through a 63-µm sieve. Samples were rinsed with methanol and then dried on a hot plate. The >125-µm fraction was examined for the planktonic foraminifers, and the 63- to 125-µm fraction was studied for the zonal markers, if they were absent in the larger size fractions.

The abundance of planktonic foraminifers is defined as follows:

Table 1. Cenozoic calcareous nannofossil datums used for Leg 149.

Event	Calibration	Age (Ma)	Zone (base)
BA. *Emiliania huxleyi*		0.08	
B. *Emiliania huxleyi*		0.26	NN21
T. *Pseudoemiliania lacunosa*		0.46	NN20
T. *Reticulofenestra* sp. A (>6.5 µm)		0.81	
B. *Gephyrocapsa omega* >4.0 µm		0.87	
B. *Gephyrocapsa omega* (>3.8 µm)	Jaramillo	0.92	
B. *Reticulofenestra sp. A* (>6.5 µm)		0.98	
T. *Gephyrocapsa* spp. >5.5 µm		1.10	
T. *Hellicosphaera sellii*		1.12	
B. *Gephyrocapsa* spp. >5.5 µm		1.37	
T. *Calcidiscus macintyrei* (cir., ≥10 µm)		1.47	
T. *Calcidiscus tropicus* (cir., ≥11.5 µm)		1.54	
B. *Gephyrocapsa oceanica* ≥4.0 µm		1.58	
B. *Gephyrocapsa caribbeanica*		1.64	
T. *Discoaster brouweri*	Olduvai	1.88	NN19
BA. *Discoaster triradiatus*		2.12	
T. *Discoaster pentaradiatus*	Matuyama	2.27	NN18
T. *Discoaster surculus*		2.40	NN17
T. *Discoaster tamalis*	Gauss	2.60	
T. *Sphenolithus neoabies*	Gilbert	3.45	
T. *Reticulofenestra pseudoumbilica*	Gilbert	3.56	NN16
B. *Discoaster tamalis*		3.80	
T. *Sphenolithus abies*		3.86	
BA. *Discoaster asymmetricus*	Gilbert	3.87	
TA. *R. pseudoumbilica/Sphenolithus abies*		4.10	
B. *Pseudoemiliania lacunosa*		4.00	
T. *Amaurolithus tricorniculatus*		4.26	NN15
T. *Ceratolithus acutus*	Sidufjall	4.43	
B. *Ceratolithus rugosus*	Thvera	4.90	NN13
B. *Ceratolithus acutus*	Gilbert	5.17	
T. *Triquetrorhabdulus rugosus*	Gilbert	5.30	
T. *Discoaster quinqueramus*	Gilbert	5.38	NN12
T. *Amaurolithus primus*		5.54	
T. *Amaurolithus amplificus*	C3A	6.01	
B. *Amaurolithus amplificus*	C3A	6.34	
B. *Amaurolithus primus*	C3B/C4	7.01	NN11
B. *Discoaster quinqueramus*	C4	7.60	
B. *Discoaster berggreni*	C4	8.28	NN11
T. *Discoaster bollii*		8.38	
T. *Discoaster hamatus*	C4A	8.85	NN10
T. *Catinaster* spp.	C4A	9.00	
B. *Discoaster hamatus*	C5	10.00	NN9
B. *Catinaster calyculus*	C5	10.00	
T. *Coccolithus miopelagicus*	C5	10.22	
B. *Catinaster coalitus*		11.50	NN8
T. *Cyclicargolithus floridanus*		11.71	
B. *Discoaster kugleri*	C5A	12.20	NN7
B. *Triquetrorhabdulus rugosus*	C5A	12.50	
T. *Coronocyclus nitescens*	~C5A/C5AA	12.80	
T. *Sphenolithus heteromorphus*	C5AB	13.37	NN6
T. *Helicosphaera ampliaperta*	C5B	16.00	NN5
TA. *Discoaster deflandrei*	C5B	16.05	
B. *Sphenolithus heteromorphus*	C5D	18.42	
T. *Sphenolithus belemnos*	C5E	18.80	NN4
B. *Sphenolithus belemnos*	C6	19.40	
T. *Triquetrorhabdulus carinatus*			NN3
B. *Discoaster druggii*	C6C	22.80	NN2
TA. *Sphenolithus delphix*		22.80	
T. *Reticulofenestra bisecta*		23.30	
BA. *Sphenolithus delphix*		24.50	
T. *Sphenolithus ciperoensis*	C6C/C7	24.60	
T. *Helicosphaera recta*	C6C	24.70	NN1
T. *Sphenolithus distentus*	C9	27.60	NP25
B. *Sphenolithus ciperoensis*	C10	29.40	NP24
B. *Sphenolithus distentus*		33.10	
T. *Reticulofenestra umbilica*	C12	33.70	NP23
T. *Cyclicargolithus formosus*	C12	34.00	NP22
T. *Discoaster saipanensis*	C13	35.60	NN21
T. *Discoaster barbadiensis*	C13	35.60	
B. *Isthmolithus recurvus*	C15	37.10	NP19
B. *Chiasmolithus oamaruensis*	C16	38.40	NP18
T. *Chiasmolithus solitus*	C18	40.80	NP17
T. *Blackites gladius*	C20	44.40	NP16
B. *Nannotetrina alata*	C21	48.10	NP15
B. *Discoaster sublodoensis*	C22	50.80	NP14
B. *Discoaster lodoensis*	C23	54.00	NP12
T. *Tribrachitus contortus*	C24	55.20	NP11
B. *Discoaster multiradiatus*	C25	57.50	NP9

Notes: T. = top; B. = bottom; BA. = bottom acme; TA. = top acme. Ages are from Berggren, Kent, and van Couvering (1985); Berggren et. al. (1985); Berggren, Kent, and Flynn (1985); Gartner (1990), and de Kaenel (unpubl. data) and have been recalibrated with the paleomagnetic time scale of Harland et al. (1990).

B (barren);
R (rare) = <10 specimens;
F (few) = 10-100 specimens;
C (common) = 101-500 specimens; and
A (abundant) = >500 specimens.
Preservation characteristics were divided into three categories:

P (poor) = almost all specimens were dissolved or broken and fragments dominated;
M (moderate) = 30%-90% of specimens showed dissolved or broken chambers; and
G (good) = >90% of specimens were well preserved and unbroken.

Benthic Foraminifers

The abundance of benthic foraminifers is defined as follows:

B (barren);
R (rare) = <10 specimens;
C (common) = 10-100 specimens; and
A (abundant) = > 100 specimens.

The three classes of preservation of benthic foraminifers were the same as those for the planktonic foraminifers.

Table 2. Cenozoic planktonic foraminifer datums used for Leg 149.

Event	Age (Ma)	Range	Zone (base)
T. *Globigerinoides fistulosus*	1.6		
T. *Globigerinoides obliquus extremus*	1.8	1.16–1.90	
B. *Globorotalia truncatulinoides*	1.9	1.5–1.9	N22
T. *Globoquadrina altispira*	2.9	2.8–2.99	
B. *Globigerinoides fistulosus*	2.9		
T. *Sphaeroidinellopsis* spp	3.0	2.90–3.04	N21
B. *Globorotalia tosaensis*	3.1		
T. *Pulleniatina primalis*	3.5		
T. *"Globigerina" nepenthes*	3.9	3.96–4.7	
B. *Globorotalia crassaformis*	4.3		
B. *Sphaeroidinella dehiscens*	5.1		N19
B. *Globorotalia tumida*	5.2		N18
B. *Globigerinoides conglobatus*	5.3		
T. *Globoquadrina dehiscens*	5.3		
B. *Pulleniatina primalis*	5.8		
B. *Neogloboquadrina humerosa*	7.5		
B. *Globorotalia plesiotumida*	9.0	8.8–9.3	
B. *Neogloboquadrina acostaensis*	10.2	10.1–10.3	N16
T. *Globorotalia siakensis*	10.4		N15
B. *"Globigerina" nepenthes*	11.3		N14
B. *Sphaeroidinellopsis subdehiscens*	11.8		N13
B. *Globorotalia fohsi lobata*	13.1		
B. *Globorotalia praefohsi*	14.0		N11
B. *Globorotalia peripheroacuta*	14.6		N10
B. *Orbulina suturalis*	15.2		N9
B. *Praeorbulina sicana*	16.3		N8
T. *Catapsydrax dissimilis*	17.6		N7
B. *Globigerinatella insueta*	17.9		N6
T. *Globorotalia kugleri*	20.1		N5
B. *Globoquadrina dehiscens*	21.2		
B. *Globorotalia kugleri*	23.7		"N4"
B. *Globigerinoides primordius*	24.2		
T. *Paragloborotalia opima*	27.5		P22
T. *Globigerina ampliapertura*	30.8		P21
T. *Pseudohastigerina*	33.0		P20
T. Hantkeninids, *Globigerinatheka*	35.4		P18
B. *Globigerina tapuriensis*	35.4		
T. *Turborotalia cerroazulensis* Group	36.5		
T. *Acarinina*	39.9		P15
T. *Orozovella spinulosa*	40.6		
B. *Globigerinatheka semiinvoluta*	40.8		
T. *Globigerinatheka beckmanni*	41.1		P14
T. *Morozovella aragonensis*	44.6		P12
B. *Hantkenina*	50.0		P10
B. *Morozovella formosa*	54.7		P7
T. *Morozovella velascoensis*	56.8		
T. *Planorotalites pseudomenardii*	57.5		P5
B. *Planorotalites pseudomenardii*	59.8		P4
B. *Morozovella pusilla*	60.2		P3b
B. *Morozovella conicotruncata*	60.2		P3b
T. *Morozovella angulata*	60.6		P3a

Notes: T. = top; B. = bottom. Ages are from Berggren, Kent, and van Couvering (1985), Berggren et al. (1985), and Berggren, Kent, and Flynn (1985) and have been calibrated with the paleomagnetic time scale of Harland et al. (1990).

Paleobathymetric Methods

Benthic foraminifers were examined from the >63-µm size fraction. Paleobathymetry estimated using the smaller benthic foraminifers was primarily based on van Morkhoven et al.'s (1986) depth zonations. Bathymetric ranges are as follows: neritic (0-200 m) is divided into upper (0-30 m), middle (30-100 m), and lower (100-200 m); bathyal is divided into upper (200-600 m), middle (600-1000 m), and lower (1000-2000 m); and abyssal (>2000 m).

PALEOMAGNETISM

Paleomagnetic studies performed aboard the *JOIDES Resolution* during Leg 149 included routine measurements of natural remanent magnetization (NRM) and of magnetic susceptibility of sedimentary, volcanic, and basement material. The measurement of magnetic remanence generally was accompanied by alternating field (AF) or thermal demagnetization to remove secondary magnetization. Details of the laboratory instruments and configurations are given in the "Explanatory Notes" chapter for Leg 145 (Shipboard Scientific Party, 1993c).

Remanent Magnetization Measurements

Remanence measurements of sediments and rocks were performed by passing continuous archive-half core sections through the cryogenic magnetometer. The ODP core orientation scheme arbitrarily designates the positive X-axis direction as the in-situ horizontal direction from the center of the core to the median line between a pair of lines scribed lengthwise on the working half of each core liner. The maximum AF demagnetizing field allowed by the Information Handling Panel for archive-half sections is 15 mT or the median destructive field, whichever is lower. In some cores, this field is insufficient to remove secondary remanence and isolate the primary component of remanence required for magnetostratigraphy and leg objectives. Therefore, at least one discrete shipboard paleomagnetic sample was taken from each section and from each representative lithology. These samples were demagnetized using either the Schonstedt GSD-1 AF demagnetizer or the Schonstedt thermal demagnetizer.

Discrete samples were taken from soft sediment using oriented standard plastic boxes (6 cm^3). To reduce the deformation of the sediment, the core was cut using a thin stainless steel spatula before pressing the plastic sampling boxes into the sediment. Minicores were drilled from lithified sedimentary rocks and igneous rocks using a water-cooled nonmagnetic drill bit attached to the standard drill press.

Low-field Susceptibility

Whole-core susceptibility measurements are relatively rapid to make, are nondestructive, and provide an indication of the amount of magnetizable material in the sediment, including ferrimagnetic and paramagnetic constituents. Whole-core volume magnetic susceptibility was measured using the automated MST. Measurements were performed usually every 5 cm at the low sensitivity range (1.0) and in the SI mode. The susceptibility response is a function of the mineralogy as well as the shape and volume of the magnetic particles within the rocks. Because magnetic susceptibility is a temperature-dependent property, the cores were permitted to equilibrate thermally

(2-4 hr) prior to measurement. The general trend of the susceptibility curve was used to characterize both the magnetic material in the sediment cores, as well as subtle environmental and geologic changes within the sediments.

Core Orientation

Core orientation of the advanced hydraulic piston (APC) cores was achieved with an Eastman-Whipstock multishot tool and the new Tensor multishot tool, both of which are rigidly mounted on a nonmagnetic sinker bar. The Eastman-Whipstock tool consists of a magnetic compass and a small camera. The battery-operated camera takes photographs at prescribed intervals from 0.5 to 2 min from the time it leaves the deck. At the bottom of the hole, the core barrel is allowed to rest for sufficient time (2-8 min) to permit the compass needle to settle and to make sure that several photographs are taken before the corer is shot into the sediment.

The Tensor tool consists of three mutually perpendicular magnetic sensors and two perpendicular gimbals. The information from both sets of sensors allows the azimuth and dip of the hole to be measured, as well as the azimuth of the double orientation line on the core liner.

Magnetostratigraphy

Where magnetic cleaning successfully isolates the primary component of remanence, paleomagnetic inclinations are used to assign a magnetic polarity to the stratigraphic column. With the assistance of biostratigraphic data, we attempted an interpretation of the magnetic polarity stratigraphy in the site chapters. During Leg 149, we adhered to the chronostratigraphic nomenclature and geochronology of Harland et al. (1990; see Table 3 and Figs. 5 to 7). For the Neogene, we used the revised ages of geomagnetic reversal boundaries taken from the new magnetic polarity time scale of Cande and Kent (1992).

Table 3. Chronostratigraphic nomenclature and geochronology of Harland et al. (1990), used during Leg 149.

Anomaly	Normal polarity interval (Ma)	
1	0.00	0.78
1R-1	0.91	0.97
2	1.65	1.88
2R-1	2.06	2.09
2A	2.45	2.91
2A	2.98	3.07
2A	3.17	3.40
3.1	3.87	3.99
3.2	4.12	4.26
3.2R-1	4.41	4.48
3.3	4.79	5.08
3A	5.69	5.96
3A	6.04	6.33
3B	6.66	6.79
4	7.01	7.10
4	7.17	7.56
4	7.62	7.66
4A	8.02	8.29
4AR-1	8.48	8.54
4AR-2	8.78	8.83
5	8.91	9.09
5	9.14	9.48
5	9.49	9.80
5	9.83	10.13
5	10.15	10.43
5R-1	10.57	10.63
5R-2	11.11	11.18
5A.1	11.71	11.90
5A.2	12.05	12.34
5AR-1	12.68	12.71
5AR-2	12.79	12.84
5AA	13.04	13.21
5AB	13.40	13.64
5AC	13.87	14.24
5AD	14.35	14.79
5B.1	14.98	15.07
5B.2	15.23	15.35
5C	16.27	16.55
5C	16.59	16.75
5C	16.82	16.99
5D	17.55	17.87
5DR-1	18.07	18.09
5E	18.50	19.00
6	19.26	20.23
6A.1	20.52	20.74
6A.2	20.97	21.37
6AA	21.60	21.75
6AAR-1	21.93	22.03
6B	22.23	22.60
6C.1	22.90	23.05
6C.2	23.25	23.38
6C.3	23.62	23.78
7	25.01	25.11
7	25.17	25.45
7A	25.84	26.01
8	26.29	26.37
8	26.44	27.13
9	27.52	28.07
9	28.12	28.51
10	29.00	29.29
10	29.35	29.58
11	30.42	30.77
11	30.82	31.21
12	31.60	32.01
13	34.26	34.44
13	34.50	34.82
15	36.12	36.32
15	36.35	36.54
15A	36.93	37.16
16	37.31	37.58
16	37.63	38.01
17	38.28	39.13
17	39.20	39.39
17	39.45	39.77
18	39.94	40.36
18	40.43	40.83
18	40.90	41.31
19	42.14	42.57
20	43.13	44.57
21	47.01	48.51
22	50.03	50.66
23	51.85	52.08
23	52.13	52.83
23R-1	53.15	53.20
24	53.39	53.69
24	54.05	54.65
25	57.19	57.80
26	58.78	59.33
27	61.65	62.17
28	62.94	63.78
29	64.16	64.85
30	65.43	67.14
31	67.23	68.13
32.1	70.14	70.42
32.2	70.69	72.35
32R-1	72.77	72.82
33	73.12	79.09
34	83.00	124.32
M1	124.88	127.35
M2	127.70	128.32
M4	130.17	131.05
M6N	131.51	131.64
M7N	131.74	131.89
M8N	132.25	132.53
M9N	132.75	132.99
M10N	133.41	133.72
M10NN	134.01	134.31
M10NN	134.36	134.65
M10NN	134.67	134.94
M11N	135.17	135.87
M11-1N	136.27	136.31
M11AN	136.64	137.30
M12N	137.37	137.63
M12-2N	138.28	138.36
M12AN	138.53	138.82
M13N	138.92	139.14
M14N	139.50	139.73
M15N	140.46	141.02
M16N	141.47	142.76
M17N	143.28	143.61
M18N	144.80	145.25
M19N	145.58	145.69

IGNEOUS AND METAMORPHIC PETROLOGY AND GEOCHEMISTRY

Core Curation and Shipboard Sampling

Before splitting igneous and metamorphic rock cores, the whole cores were examined for structural features. Sediments in contact with the hard rocks were examined for evidence of chilling, baking, and alteration. Contiguous pieces of core were numbered sequentially from the top of each core section and labeled according to standard ODP procedures. Cores were split in such a way as to allow important features and structures to be represented in both the working and archive samples. The archive half was described on the visual core description (VCD) form and was photographed before storage. Only the working half was sampled.

Visual Core Descriptions of Igneous Rocks

The standard visual core description forms were used to document the location of samples taken from the igneous rock cores (see "Cores" section, this volume) using the following notation: XRD = X-ray diffraction analysis; XRF = X-ray fluorescence analysis; TSB = petrographic thin section. When describing sequences of rocks, the core was subdivided into lithologic units on the basis of changes in texture, grain size, mineral occurrence and abundance, rock composition, and rock clast type. Rocks for which the protolith is completely obscured by metamorphism were given separate lithological names, whereas the prefix "meta" or the term "altered" is used as a modifier with the name of an identifiable protolith. We reserved the termed "altered" for igneous rocks that contain only those secondary minerals consistent with low-temperature seafloor alteration (e.g., calcite, phillipsite, celadonite, nontronite, amorphous iron oxide). When describing the relative proportion of primary and secondary minerals, the general term "alteration" was used to include all secondary minerals. Descriptive information recorded in the database (HARVI) for coarse- and fine-grained rocks:

1. The leg, site, hole, core number, core type, and section number.
2. The unit number (consecutive downhole), position in the section, number of pieces of the same lithologic type, the rock name, and the identification of the describer.
3. The Munsell color of the dry rock and the presence and character of any structural fabric including deformation.

4. The number of mineral phases visible with a hand lens and their distribution within the unit, together with the following information for each phase: (a) abundance (volume %); (b) size range in mm; (c) shape; (d) degree of alteration; and (e) further comments.

5. The groundmass texture: glassy, fine grained (<1 mm), medium grained (1-5 mm), or coarse grained (>5 mm). Grain size changes within units were also noted.

6. The presence and characteristics of secondary minerals and alteration products.

7. The relative amount of rock alteration was described in the rock description. Rocks were classified as fresh (<2%); slightly altered (2%-10%); moderately altered (10%-40%); highly altered (40%-80%); very highly altered (80%-95%); and completely altered (95%-100%). The type, form, and distribution of alteration was also noted.

8. The presence of veins and fractures, including their abundance, width, mineral fillings or coatings, orientation, and associated wall rock alteration. The hade of veins and fractures with respect to the core axis was measured with a protractor (see "Structural Geology" section, this chapter). The relationship of the alteration and vein filling minerals with respect to veins and fractures also was noted. Vein networks and their mineralogy were indicated adjacent to the graphic representation of the archive half.

9. Other comments, including notes on the continuity of the unit within the core and on the interrelationship of units.

Fine-grained Volcanic Rocks

Basalt is called aphyric (<1%), sparsely phyric (1%-2%), moderately phyric (2%-10%), or highly phyric (>10%), depending upon the proportion of phenocrysts visible with the hand lens and binocular microscope. Basalts are further described by phenocryst type (e.g., a moderately plagioclase-olivine phyric basalt contains 2%-10% phenocrysts, mostly plagioclase, with subordinate olivine). The abundance of vesicles, their shape, and type of mineral fillings were also noted. More specific rock names were given where chemical analyses or thin sections were available.

Brecciated Rocks

A breccia is defined as any rock composed of angular broken rock fragments held together by finer fragments or glassy material. They form in many ways including volcanic, hydraulic, tectonic, and impact. Volcanic breccias form as accumulated volcanic gases expand suddenly producing a chaotic array of differently sized angular volcanic fragments which may be welded and altered at high temperature. Hydraulic breccias form as accumulated water vapor expands suddenly to produce a chaotic array of different sized angular fragments, perhaps welded and altered at low temperature. Tectonic breccias form along fault or shear zones during displacement, producing angular fragments that moved along the fault zone. The explosive volcanic and hydraulic breccias would typically have random chaotic collections of angular fragments, whereas tectonic breccias would typically have irregular fragments concentrated along two-dimensional planar fault surfaces. A large range of fragment sizes would be expected in explosive breccias relative to fault breccia.

Coarse-grained Plutonic Rocks

The texture of plutonic igneous rocks was described in terms of crystallinity, granularity (the absolute and the relative sizes of crystals), crystal shapes, and crystal arrangement. Rock names were assigned according to essential primary minerals using a triangular diagram and based on the primary minerals being either plagioclase, olivine, orthopyroxene, or clinopyroxene (Fig. 9). Genetically significant accessary minerals were used to modify the rock name further

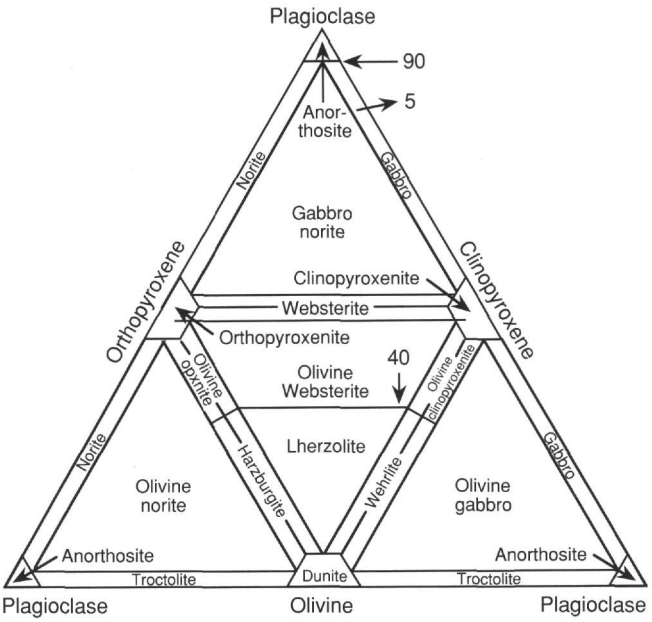

Figure 9. Classification of plutonic igneous rocks having a primary mineralogy consisting of plagioclase, olivine, orthopyroxene, or clinopyroxene.

(e.g., spinel or plagioclase lherzolite). The ranges of grain size in the plutonic rocks were recorded using the terms: very coarse-grained (crystal diameters >30 mm), coarse-grained (crystal diameters of 5-30 mm), medium-grained (crystal diameters of 1-5 mm), and fine-grained (crystal diameters of <1 mm).

Oxide and sulfide minerals were classified on the basis of type and texture and, where possible, identified as of primary or secondary origin. The percentage of these minerals was visually estimated, and individual minerals were typically undifferentiated in hand specimen. Iron oxide staining was recorded on partially altered minerals and along fractures. The texture of the oxide and sulfide minerals was described in terms of the size, shape, and orientation of the mineral and its relationship with adjacent minerals. Their form was generally described as euhedral, subhedral, or anhedral.

Textural and mineralogical variations were recorded, noting the interval over which a particular feature was observed, and its relation to other features. Modally graded zones were defined as those where the primary mineralogy showed gradational changes in grain size. Texturally graded zones were defined as those where a gradational change in texture was observed (e.g., from poikilitic to granular). The direction of grading was related to stratigraphic position. Crystal alignment of probable igneous origin was described as planar, curved, or irregular. The orientation of any planar structure was recorded by measuring apparent dips relative to the core axis.

Alteration, Veining, and Metamorphism

Alteration, veining, and metamorphism were recorded to provide three types of data: (1) the extent of igneous mineral replacement by metamorphic or secondary minerals; (2) the extent to which metamorphic minerals contribute to subsolidus fabric; (3) the abundance, character, and orientation of veins, along with their associated haloes; and (4) the thickness and orientation of shear zones. Overprinting relationships between secondary minerals, particularly cross-cutting relationships of veins and shear zones, were reported to document the relative timing of these events. Sheared rocks were described as my-

lonites, cataclasites, or porphyroclastites, depending on the extent to which crushing, recrystallization, and fabric development had modified the primary igneous rock. Identification of vein-filling material was frequently checked using XRD.

Individual vein types were identified by color and mineralogy. Data on abundance, width (mm), orientation, and texture and abundance of vein-filling minerals were recorded for each piece containing one or more veins. In pieces having numerous veins, sequences, and patterns produced by intersecting veins and sequences of changing mineralization in the veins were recorded and described.

Thin-section Descriptions

Thin sections of igneous rocks were examined to complement and refine hand-specimen observations. The same terminology was used for thin-section and visual-core descriptions. The percentages and textural descriptions of individual phases were recorded using a computerized database (HRTHIN). Thin-section descriptions are included in the "Cores" section (this volume) as separate tables for each core.

X-ray Diffraction Analyses

A Philips ADP 3520 X-ray diffractometer was used for the X-ray diffraction (XRD) analysis of mineral phases. Ni-filtered CuKα radiation generated at 40 kV and 35 mA was used. Peaks were scanned from a 2θ of 2° to 32°, with a step size of 0.02°, and a counting time of 2 sec/step.

Samples were ground to <200 µm mesh in a Spex 8000 Mixer Mill using tungsten carbide and steel. The powder then was pressed into aluminum sample holders or smeared onto glass plates for analysis. Diffractograms were interpreted with the help of a computerized search and match routine using the Joint Committee on Powder Diffraction Standards powder files.

X-ray Fluorescence Analysis

Before analysis, samples were crushed in a Spex 8510 shatterbox using a tungsten carbide barrel. Where recovery permitted, at least 20 cm^3 of material was ground to ensure a representative sample. The tungsten carbide barrel was used despite the considerable W contamination and minor Ta, Co, and Nb contamination, which makes the powder unsuitable for later instrumental neutron activation analysis (INAA).

A fully automated wavelength-dispersive ARL8420 XRF (3 kW) system, equipped with an Rh-target X-ray tube, was used to determine the abundances of major and trace elements in whole-rock samples (Table 4). Analyses of the major oxides were performed on lithium borate glass disks doped with lanthanum as a "heavy absorber" (Norrish and Hutton, 1969). The disks were prepared from 500mg of rock powder that had been ignited for 2 hr at about 1030°C and mixed with 6.000 g dry flux (pre-weighed onshore) consisting of 80% lithium tetraborate and 20% La_2O_3. This mixture then was melted in air at 1150°C in a Pt-Au crucible for about 10 min and poured into a Pt-Au mold using a Claisse fluxer. The 12:1 flux-to-sample ratio and the use of the lanthanum absorber made matrix effects insignificant over the normal range of igneous rock compositions. Hence, the relationship between X-ray intensity and concentration becomes linear and can be described by:

$$C_i = (I_i \times m_i) - b_i, \quad (1)$$

where C_i = concentration of element i (wt%); I_i = peak X-ray intensity of element i; m_i = slope of calibration curve for element i (wt%/counts/second); and b_i = apparent background concentration for element i (wt%).

The slope m_i was calculated from a calibration curve derived from the measurement of well-analyzed reference rocks, such as BEN, BR, and DRN from Geostandards, France; BHVO-1, RGM-1, and AGV-1 from the U.S. Geological Survey; JGB-1 and JP-1 from the Geological Survey of Japan; AII-92-29-1 from Woods Hole Oceanographic Institution/Massachusetts Institute of Technology; and K1919 from Lamont-Doherty Earth Observatory. Two other standard reference rocks were run with samples as unknowns. A complete list of analyses for the standards used to derive calibration curves is given in Tables 5 (major elements) and 6 (trace elements). The background b_i was determined by regression analysis from the calibration curves.

Table 4. X-ray spectrograph analytical conditions for Leg 149.

Oxide or element	Line	Crystal	Detector	Collimator	Peak angle (deg)	Background offset (deg)	Total peak (s)	Count time background (s)
SiO_2	Kα	PET(002)	FPC	Coarse	109.28	0	40	0
TiO_2	Kα	LiF(200)	FPC	Fine	86.11	0	40	0
Al_2O_3	Kα	PET(002)	FPC	Coarse	145.12	0	100	0
Fe_2O_3	Kα	LiF(200)	FPC	Fine	57.47	0	40	0
MnO	Kα	LiF(200)	FPC	Fine	62.92	0	40	0
MgO	Kα	TLAP	FPC	Coarse	44.89	± 0.80	150	300
CaO	Kα	LiF(200)	FPC	Coarse	113.09	0	40	0
Na_2O	Kα	TLAP	FPC	Coarse	54.72	–1.20	150	150
K_2O	Kα	LiF(200)	FPC	Coarse	136.62	0	100	0
P_2O_5	Kα	Ge(111)	FPC	Coarse	141.87	0	100	0
Nb	Kα	LiF(200)	Scint	Fine	21.40	–0.35	200	100
Zr	Kα	LiF(200)	Scint	Fine	22.55	–0.35	100	50
Y	Kα	LiF(200)	Scint	Fine	23.76	–0.40	100	50
Sr	Kα	LiF(200)	Scint	Fine	25.15	–0.40	100	50
Rb	Kα	LiF(200)	Scint	Fine	26.62	–0.60	100	50
Zn	Kα	LiF(200)	Scint	Coarse	41.82	–0.40	100	50
Cu	Kα	LiF(200)	Scint	Coarse	45.06	–0.40	100	50
Ni	Kα	LiF(200)	Scint	Coarse	48.67	–0.60	100	50
Cr	Kα	LiF(200)	FPC	Fine	69.36	–0.50	100	50
TiO_2	Kα	LiF(200)	FPC	Fine	86.11	+0.50	40	20
V	Kα	LiF(200)	FPC	Fine	123.04	–0.50	100	50
Ce	Lα	LiF(220)	FPC	Coarse	128.13	1.50	100	50
Ba	Lß	LiF(220)	FPC	Coarse	128.75	1.50	100	50

Notes: Total Fe as Fe_2O_3*. FPC = Flow proportional counter using P10 gas; Scint = NaI scintillation counter. Major elements analyzed under vacuum using goniometer 2 at generator settings of 30 kV and 80 mA. Trace elements analyzed under vacuum using goniometer 2 at generator settings of 60 kV and 50mA.

Systematic errors resulting from short- or long-term fluctuations in X-ray tube intensity and instrument temperature were addressed by counting an internal standard between no more than six unknowns in any given run. The intensities of this standard were normalized to its known values, thereby providing correction factors for the measured intensities of the unknowns. To reduce shipboard weighing errors, two glass disks were prepared for each sample. Accurate weighing was difficult on board the moving platform of the *JOIDES Resolution,* and was performed with particular care as weighing errors could be a major source of imprecision in the final analysis. Five weight-measurements that agreed to within 0.5 mg (±0.1%) were taken for each sample, and the average was used as the true weight. Loss on ignition was determined by drying the sample at 110°C for 8 hr and then by weighing before and after ignition at 1030°C in air.

Trace elements were determined on pressed-powder pellets prepared by pressing (with 7 MPa of pressure) a mixture of 5.0 g of dry rock powder (dried at 110°C for >2 hr) and 30 drops of polyvinyl alcohol binder into an aluminum cap. A modified Compton scattering technique, based on the intensity of the Rh Compton peak, was used for matrix absorption corrections (Reynolds, 1967).

Replicate analyses of rock standards showed that the major-element data are precise to within 0.5% to 2.5% and are considered accurate to approximately 1 % for Si, Ti, Fe, Ca, and K, and between 3% and 5% for Al, Mn, Na, and P. The trace-element data are considered accurate to between 2% and 3% or 1 ppm (whichever is greater) for Rb, Sr, Y, and Zr, and between 5% and 10% or 1 ppm (whichever is greater) for the other elements. The accuracy of Ba and Ce is considerably less, and they are reported primarily for purposes of internal comparison. Precision is within 3% for Ni, Cr, and V at concentrations >100 ppm, but 10% to 25% at concentrations <100 ppm.

STRUCTURAL GEOLOGY

Introduction

The structural study of rocks sampled during Leg 149 was devoted to understanding the mechanisms of extension of the continental lithosphere during a rifting episode. Synrift-related deformation is recorded in the basement rocks and the synrift sedimentary sequences. However, structural features present in the basement rocks may have been inherited from older tectonic events, and later events must be invoked to explain structures in the post-rift sequences cored during Leg 149.

This section deals with the macroscopic and microscopic descriptions of sediment and basement rock cores. The intention of this record is to identify and describe in a systematic and, if possible, a quantitative way the structural features in the cores and their orientation. The method used here is derived from that used during previous legs (Leg 131, Taira, Hill, Firth, et al., 1991; Leg 134, Collot, Greene, Stokking, et al., 1992; Leg 140, Dick, Erzinger, Stokking, et al., 1992; Leg 141, Behrmann, Lewis, Musgrave, et al., 1992).

Macroscopic Core Description

Structures were measured on the face of the archive half or the working half of the split core, depending on the availability of the cores at the time of description. Initial data were recorded graphically section-by-section on a scaled structural visual core description form (VCD). The location of a structure was recorded in centimeters from the top of the section, according to ODP convention. Where a structure extended over an interval, the top and bottom of its range were recorded. More detailed information, particularly the orientation of

Table 5. Accepted compositions of the international rock standards used for analyzing major elements.

Standard	SiO_2 (wt%)	TiO_2 (wt%)	Al_2O_3 (wt%)	Fe_2O_3 (wt%)	MnO (wt%)	MgO (wt%)	CaO (wt%)	Na_2O (wt%)	K_2O (wt%)	P_2O_5 (wt%)	Total
BHVO	49.62	2.68	13.67	12.23	0.17	7.21	11.32	2.17	0.53	0.27	99.87
G2	69.52	0.50	15.25	2.70	0.03	0.77	1.98	4.10	4.52	0.14	99.51
BR	39.40	2.69	10.50	13.29	0.21	13.70	14.22	3.13	1.45	1.07	99.66
DRN	53.97	1.10	17.86	9.86	0.22	4.43	7.18	3.04	1.73	0.24	99.63
AGV	59.93	1.06	17.26	6.84	0.10	1.54	4.97	4.45	2.95	0.50	99.60
JGB-1	43.99	1.64	17.89	15.35	0.17	7.93	12.13	1.25	0.26	0.05	100.66
AII-92	49.34	1.75	15.49	10.85	0.18	7.51	11.16	3.07	0.17	0.16	99.68
K1919	49.73	2.83	13.75	12.21	0.18	6.83	11.32	2.35	0.53	0.28	100.01
UBN	44.93	0.13	3.30	9.50	0.14	40.12	1.36	0.00	0.02	0.05	99.55
RGM-1	74.58	0.28	13.82	1.89	0.04	0.29	1.17	4.12	4.35	0.05	100.59
BIR	48.04	0.96	15.53	11.34	0.18	9.71	13.34	1.82	0.03	0.02	100.97
BEN	39.58	2.70	10.43	13.30	0.21	13.62	14.37	3.30	1.44	1.09	100.04
JB-2	53.40	1.19	14.73	14.39	0.20	4.68	9.93	2.04	0.43	0.10	101.09
JB-3	51.16	1.45	16.93	11.91	0.16	5.21	9.88	2.83	0.80	0.29	100.62
GH	76.36	0.09	12.73	1.38	0.05	0.05	0.72	3.84	4.79	0.01	100.02

Table 6. Accepted compositions of the international rock standards used for analyzing trace elements.

Standard	Nb (ppm)	Zr (ppm)	Y (ppm)	Sr (ppm)	Rb (ppm)	Zn (ppm)	Cu (ppm)	Ni (ppm)	Cr (ppm)	TiO_2 (ppm)	V (ppm)	Ce (ppm)	Ba (ppm)
AGV	15	231	19	656	67	84	59	16	11	1.05	121	67	1208
UBN			2.4	7.40	3.5	92	28	2000	2300	0.27	75		30
G2	12	300	9	480	170	85	11	4	9	0.48	36	159	1885
BHVO	19	180	26	420	10	113	140	120	300	2.71	310	38	127
RGM	9.5	200	22	100	155	35	11	6	4	0.27	13	49	800
DRN	9	125	30	400	70	145	50	16	40	1.06	225		50
GH	84	145	80	10	392	85	14	4	6	0.08	4	70	22
BEN	173	265	30	1370	47	120	72	267	360	2.61	235	152	1025
STM	270	1260	53	730	120	230	4	2.1		0.15	2	260	590
BR	105	270	30	1320	47	85	72	268	346	2.61	240	148	1060
BIR	2.3	18	16	107		70	125	166	373	0.96	312	1.6	6
JB-2	0.8	50	26	178	18	110	230	14	27	1.17	578	7	
JB-3	2.3	100	26	395	27	95	197	39	53	1.40	383	21	
JA-1	4	89	27	266	13	96	44	2	14	0.87	105	22	17

Tectonic feature identifiers						
Identifier	ID	Planar component	ID	Linear components	ID	Comments
"Cold" deformation:						
Fault	Fa	Fault plane	Fa	Slickenline	sl	Any discrete planar break showing a displacement. Where possible, sense of movement is recorded in the core face (normal or inverse), or at the core ends (dextral or sinistral).
Fracture or gash–mineral vein	Fr–V	Fracture or gash plane–mineral vein	Fr–V			Any discrete planar break showing no clear displacement. Openings filled with mineral or minerals such as calcite (Vc), serpintine (Vs), sulfide (Vp), chlorite (Vch), or epidote (Vep).
Fracture cleavage	Fc					Organized fracture network.
Schistosity	S2					Penetrative low temperature shear deformation expressed as (a) schistosity, associated with intense fracture cleavage, or C–S fabric and/or local brecciation, or (b) foliation in sheared breccia.
Schistosity	S3					Shear zone in Site 899 breccia and in interbedded sediments.
Breccia	B					Generally tectonic breccia resulting from intense fracturing (cataclasite).
"Hot" deformation:						
Primary layering	PL					In ultrabasites, marked by bands enriched in pyroxene, in surrounding peridotite.
Primary foliation	PF					In ultrabasites, marked by elongated spinel and plagioclase.
Fabrics		Foliation	S	Lineation	L	Any plane or line on this plane of preferential orientation of minerals.
Intrusive dykes or veins	D	Intrusive dykes or veins	D			In igneous rocks, injected material of same or different composition that has sharp boundaries with the surrounding rock.

Figure 10. Terminology of structural identifiers used for structure observed in core during Leg 149.

structures, was recorded on a working core description form adapted from those devised during Leg 131 (Taira, Hill, Firth, et al, 1991) and on a computer spreadsheet. A numerical identifier was used to correlate individual structures between the three forms.

Description and Measurement of the Structures

The descriptive terminology for macroscopic features is listed in Figure 10. The terms may be modified by added descriptions and sketches. Natural structures often are difficult to distinguish from those caused by drilling and coring disturbance. Planar structures having polished surfaces and/or linear grooves were regarded as tectonic- rather than drilling-induced. In zones of brecciation, features were attributed to drilling disturbance if their tectonic origin was in doubt. The recommendations of Lundberg and Moore (1986, p. 42-43) were followed for the sediments.

Several problems are inherent to this study. Commonly, only part of the core associated with any one core interval is actually recovered, leading to a sampling bias that for structural purposes is particularly acute. Friable material from fault zones and low temperature shear zones in particular may be missing in cases of incomplete recovery. When faulted or fractured rock from such zones is recovered, it is often highly disturbed and its original orientation altered.

Determining the orientation of observed structures (and intrusive dikes) is difficult. First, structures were oriented relative to core reference coordinates (see below). This arbitrary reference frame will be related, if possible, to true north and true vertical using paleomagnetic, and Formation MicroScanner (FMS), data when available.

Our measurements of the orientations of structures observed in the cores were facilitated by a simple tool described in the "Explanatory Notes" chapter of Leg 131 *Initial Reports* volume (Taira, Hill, Firth, et al., 1991). The dip of a structure exposed in the split core was recorded according to the convention illustrated in Figure 11. The plane normal to the axis of the borehole was referred to as the apparent horizontal plane. On this plane, a 360° net was used with a "pseudonorth" (000°) direction defined as the bottom of the semicircular archive-half core. Thus, the face of the split core (the core face) was the plane 090°/90° (strike, dip), and the plane at right angles to the core face and parallel to the core axis was the plane 000°/90° (strike, dip). The apparent dip on the core face, either dipping toward the "east" or toward the "west" (looking at the face of the archive half of the core with its top looking upward), was measured. A second apparent dip was measured in one of the two planes, depending on exposure. Usually, we measured the dip in the plane 000°/90° at right angles to the core face, with the apparent dip direction in this plane be-

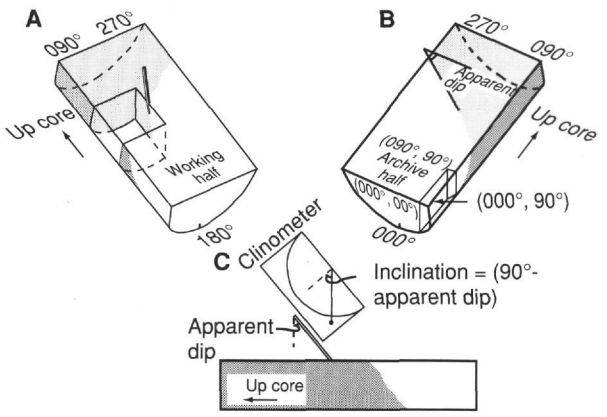

Figure 11. Conventions used for measuring azimuths and dips of structural features in the core and techniques used for measuring structural planes in three dimensions in the core reference frame. The core reference frame conventions for the working half and the archive half of the core can be seen in (A) and (B). The "E-W" (core reference frame) apparent dip of a feature was measured first and recorded as an apparent dip toward either 090° or 270° (in this case, the apparent dip is toward 090°). A second apparent dip was measured by making a cut parallel to the core axis, but perpendicular to the core face in the working half of the core (A). The feature was identified on the new surface, and the apparent dip in the "N-S" (core reference frame) direction was marked with a toothpick. The apparent dip was measured with a clinometer (C) and recorded as a value toward either 000° or 180°. In this diagram, the apparent dip is toward 180° (into the working half). True dip and strike of the surface in the core reference frame were calculated from the two apparent measurements.

ing toward "north" or "south." Sometimes, we measured the dip angle on plane 000°/00°, where the strike of the plane was recorded relative to the core reference frame. When possible, a direct measurement of the strike and dip was performed. Dips recorded at this stage were based on the assumption that the long axis of the core was vertical; that is, deviations of the hole from vertical were ignored.

The great circle of cylindrical best fit of the two apparent dips (regarded as lines) was calculated using the Stereonet plotting program of R.W. Allmendinger (version 3.5). The measurements on the core face or on plane 000°/90° were taken replacing N, E, S, and W with their azimuths, that is, 0°, 90°, 180°, and 270°, respectively. The orientation of this "best-fit great circle" provided the working azimuth and dip of the observed structure (i.e., the azimuth and dip within the core reference frame).

The orientations of linear structures were recorded as "working trends." These were measured in the direction of plunge and referred to the core reference frame in the same way as planar surfaces. In the case of some small pieces, the vertical axes could be identified from their cylindrical shape, but not the up-going direction, as they may have rolled in the core barrel. In these pieces, the true dip of planar features was recorded, but not the direction of dip, which was meaningless.

The sense of fault displacement was recorded and referred to as normal, reverse, or strike-slip with sinistral or dextral movement. The apparent magnitude of displacement was measured on the core face and/or on the top of broken pieces. Offset was normally measured on a plane normal to the displacement plane, as straight-line separation between displaced markers. Mineral and/or mylonitic foliations and lineations could be measured in much the same way as faults and veins, but as the cut surfaces were chosen to be parallel to lineations or perpendicular to foliations, they could often be measured as true orientations.

Geographic Orientation of Structures

The structures were oriented in the core reference frame, but not with respect to geographical coordinates. Re-orientation will be attempted using only paleomagnetic data, as multishot and FMS data acquired during Leg 149 are missing or of poor quality, particularly in the basement.

Paleomagnetic measurements were obtained on the core using a pass-through cryogenic magnetometer and on discrete samples taken from the core. The declination and inclination of the natural remanent magnetism (NRM), when available, can be used for orienting the structures. This method is useful on unoriented cores obtained using the RCB system, which often disrupts the core by breaking it into pieces that rotate independently of each other within the core liner. These drilling-induced rotations sometimes can be estimated and removed on the basis of the magnetic declination of the archive half, measured using the pass-through cryogenic magnetometer. This method assumes that each segment having a constant value is a homogeneous drilling piece. Paleomagnetic convention employs a "pseudonorth," or 000° direction, in the working half of the core which is 180° different from our reference frame, based on the archive half. Orientation of the structural features using magnetic data thus requires a rotation of 180° minus the magnetic declination. In some cases, a component of viscous remanent magnetization (VRM) parallel to the present-day magnetic field can be used to orient cores.

Thin-section Description

Thin-sections of basement cores recovered during Leg 149 were examined (1) to confirm macroscopic descriptions of ductile and brittle structures; (2) to determine the texture, the deformation at mineral scale, and the degree of recrystallization; (3) to provide information regarding the kinematics of high-temperature ductile deformation and the time relationship with brittle deformation; and (4) to document major structural zones and downhole textural variations. Where possible, the thin sections were oriented with respect to the core (so that the original attitude of the core axis is preserved).

ORGANIC GEOCHEMISTRY

Several organic geochemical measurements were used during Leg 149 to monitor volatile hydrocarbons and other gases as part of the shipboard safety requirements and to provide an initial characterization of the organic matter in the sediments.

Gas Sampling

Compositions of low-molecular-weight hydrocarbons and other gases were monitored in each core by the standard ODP headspace procedure (Kvenvolden and McDonald, 1986). About 5 cm^3 of sediment was obtained from the end of a freshly cut core section and placed into a 21.5-cm^3 glass serum vial. The vial was sealed with a septum and a metal crimp cap and heated at 60°C for 30 min. For each analysis by gas chromatography, a 5-cm^3 volume of gas from the headspace in the vial was extracted with a standard glass syringe.

The standard ODP vacutainer method of gas sampling (Kvenvolden and McDonald, 1986) was used whenever gas pockets or expansion voids were observed in cores as they arrived on deck. Vacutainers were pre-evacuated, septum-sealed, 20-cm^3 glass tubes. For obtaining a gas sample, a special tool was employed to penetrate the core liner.

Gas Analysis

Headspace and vacutainer gas samples were analyzed routinely using the Hach-Carle (HC) gas chromatograph. This instrument has been designed to measure, accurately and rapidly, the concentrations of methane, ethane, and propane. Ethene is resolved from ethane and can also be quantified. Samples are introduced into the HC gas chromatograph through a 1.0 cm^3 sample loop having manual column backflush. The chromatographic column was a 0.32 cm x 1.8 m stainless steel tubing packed with 80% Porapak N and Porapak Q (80/100 mesh). A flame ionization detector was used, and the chromatographic conditions were isothermal at 90°C, with helium used as carrier gas. A Hewlett-Packard 3365 ChemStation computer data collection and analysis system was used to integrate and store the results of the gas measurements.

Pyrolytic Determinations of Organic Matter Type

Two pyrolysis systems were used during Leg 149 to evaluate the type of organic matter present in sediments and sedimentary rocks: the Delsi-Nermag Rock-Eval II and the Geofina hydrocarbon meter. Both systems use whole-rock pyrolysis techniques to identify the type and maturity of organic matter and to detect petroleum potential and oil shows in sediments, as described by Espitalié et al. (1986). Sample size for both instruments was between 50 and 100 mg.

The Rock-Eval system involves a graduated temperature program that first volatilizes existing hydrocarbons at 300°C for 3 min, and then releases hydrocarbons from thermal cracking of kerogen as the temperature increases at 25°C/min from 300° to 550°C. Four parameters characterizing the organic matter are determined:

1. S_1: The amount of free hydrocarbons (bitumen) in the sample (mg hydrocarbons/g of rock) released at temperatures below 300°C.
2. S_2: The amount of hydrocarbons generated through thermal cracking of the kerogen as the sediment is heated at 25°C/min from 300° to 550°C during pyrolysis (cycle 1). S_2 is an indication of the

quantity of hydrocarbons that might have been produced in this rock, should deeper burial and greater thermal maturation have occurred.

3. S_3: The quantity of CO_2 (mg CO_2/g of rock) produced from pyrolysis of the organic matter at temperatures between 300° and 390°C.

4. T_{max}: Maturity of the organic material assessed by the temperature at which the maximum release of hydrocarbons from cracking of kerogen occurs during pyrolysis (top of the S_2 peak).

The Rock-Eval II instrument is equipped with a module that uses an algorithm and the S_1, S_2, and S_3 peak values to estimate the total amount of organic carbon (TOC) in samples.

Organic matter can be characterized from Rock-Eval data using the hydrogen index [(100 × S_2)OC], the oxygen index [(100 × S_3)OC], and the S_2/S_3 ratio. The first two parameters normally are referred to as HI and OI, respectively. Interpretations of Rock-Eval pyrolysis are considered to be unreliable for samples having less than 0.5% TOC (Katz, 1983; Peters, 1986), although a correction procedure has been described for estimating matrix effects and for obtaining reliable values from samples having lower amounts of TOC (Espitalié, 1980).

The Geofina hydrocarbon meter (GHM) employs a Varian 3400 series gas chromatograph that has been modified to include a programmable pyrolysis injector. The system has three flame ionization detectors and two capillary columns (25 m, GC2 fused silica). Like the Rock-Eval II, this tool determines S_1, the free hydrocarbons that are released up to 300°C, and S_2, the pyrolysis products that are generated from the sample kerogen. T_{max} of the S_2 peak also is determined. The effluent from the furnace is split 20:1 so that the hydrocarbon distributions making up S_1 and S_2 can be examined in detail by capillary gas chromatography. Rock-Eval and GHM parameters can be used to calculate the production index (PI) = $S_2/(S_1 + S_2)$, and petroleum potential or pyrolyzed carbon index (PC) = $0.083(S_1 + S_2)$.

Carbonate Carbon

The carbonate carbon content of samples was determined using a Coulometrics 5011 inorganic carbon analyzer (Engleman et al., 1985). A sample of about 20 mg of freeze-dried and ground material was reacted with 2N HCl. The liberated CO_2 was titrated in an ethanolamine solution containing a color indicator, and the change in color was measured by a photodetector cell. Carbonate carbon contents are expressed as weight percent $CaCO_3$, assuming all the carbonate was present as pure calcite.

Organic Carbon

The total organic carbon content (TOC) of sediment samples was determined either by the Rock-Eval TOC module or by the difference between carbonate carbon and the total carbon value determined by the Carlo Erba Model NA 1500 NCS analyzer. In the NCS analyzer, freeze-dried and ground samples were combusted at 1000°C in an oxygen stream. Nitrogen oxides were reduced to N_2, and the mixture of CO_2, SO_2, and N_2 was separated by gas chromatography and quantified with a thermal conductivity detector.

INORGANIC GEOCHEMISTRY

The shipboard analytical program for inorganic geochemistry focused solely on the chemical characterization of interstitial waters extracted from 5- to 15-cm-long whole-round sediment samples and/or taken with the in-situ sampler (the WSTP tool). During Leg 149, interstitial waters for shore-based analyses of trace elements were obtained by squeezing sediments with a plastic-lined squeezer designed by Hans Brumsack. Interstitial water samples for shipboard analysis and for ODP archives were collected either with the Brumsack squeezer or with a titanium Manheim squeezer.

The whole-round sections were cut from the core immediately after it arrived on deck and were placed in a nitrogen-filled glove bag to prevent oxidation. While in the nitrogen bag, the sediment was removed from the core liner, scraped with a plastic spatula, and loaded into the plastic-lined squeezer. Highly consolidated sediments were broken into small pieces and a portion transferred to the titanium squeezer. The sediment was squeezed at pressures up to 18,000 psi (124 MPa) in the Brumsack squeezer and up to 40,000 psi (276 MPa) in the titanium squeezer. The effluent from the Brumsack squeezer was ejected through a pre-cleaned 0.45-µm Millipore polycarbonate membrane placed inside the squeezer. In addition, the effluent was filtered through in-line pre-cleaned 0.22-µm acrodisk filters before collection in pre-cleaned syringes. The effluent from the titanium squeezer was filtered through an uncleaned 0.22-µm acrodisk filter. Effluent from each sediment sample was collected for shipboard analyses, for ODP archives, and for shore-based analyses of trace elements. The trace-element samples were transferred from the pre-cleaned plastic syringes to pre-cleaned plastic vials acidified with Ultrex HCl and stored. Samples for shipboard analyses were refrigerated, and archive samples were sealed in glass ampules.

Analytical Methods

Alkalinity and pH were determined in duplicate immediately following sample collection using the Metrohm autotitrator with a Brinkman combination pH electrode. The electrode was calibrated prior to analysis and periodically checked for drift. Salinity was estimated using a Goldberg optical hand refractometer to measure the total dissolved solids. The concentrations of the sulfate and chloride anions and the calcium, magnesium, sodium, and potassium cations were determined in duplicate using a Dionex-DX100 ion chromatograph. All samples were run at 1:200 dilution. Standards were run at the start and end of each run to test for drift in the response of the conductivity detector. Precision of separate dilutions was better than 2%. Concentrations of ammonium, silica, and phosphate were determined by the spectrophotometric techniques described in Gieskes and Peretsman (1986). Concentrations of iron, manganese, and strontium were analyzed by atomic absorption spectrophotometry (AAS).

PHYSICAL PROPERTIES

Introduction

Nondestructive measurements were made on whole sections of core using the multisensor track (MST). This incorporated the Gamma Ray Attenuation Porosity Evaluator (GRAPE), P-wave logger (PWL), and magnetic susceptibility sensors. Thermal conductivities were measured for sediments and basement rocks using the needle probe method. When the sediment was soft enough, compressional wave velocities, undrained shear strengths, and electrical resistivities were measured on the working half of the core. In addition, discrete samples were taken throughout the cores for determining index properties and compressional wave velocities.

Nondestructive Measurements

Multisensor Track

The MST incorporates the GRAPE, PWL, and magnetic susceptibility sensors. A natural gamma-ray sensor was added to the MST at the beginning of Leg 149, which was used only on selected cores for testing the instrument. Individual unsplit core sections were

placed horizontally on the MST, which moves the section past the four sensors.

The GRAPE measures bulk density at 1 cm intervals (minimum) by comparing the attenuation of gamma rays through the cores with attenuation through aluminum and water standards (Boyce, 1976). The GRAPE data are most reliable in APC and fullsized XCB and RCB cores and offer the potential of direct correlation with downhole bulk density logs. For the preliminary on-board processing, only every 20th measurement was used. Corrections were made for variations in core diameter, pore water composition, and mineralogy, following Evans and Cotterell (1970), Boyce (1976), and Lloyd and Moran (unpubl. data). For very disturbed cores, the GRAPE acquisition was turned off.

The PWL transmits a 500-kHz compressional-wave pulse through the core at a repetition rate of 1 kHz. The transmitting and receiving transducers are aligned perpendicular to the long axis of the core. A pair of displacement transducers monitors the separation between the compressional wave transducers; variations in the outside diameter of the liner therefore do not degrade the accuracy of the velocities. Measurements are taken at 3-cm intervals. Generally, only the APC and fullsized XCB and RCB cores were measured. The quality of the data was assessed by examining the arrival time and amplitude of the received pulse. Data having anomalously large traveltimes or low amplitudes were discarded.

Magnetic susceptibility was measured on all sections at intervals of 3 to 5 cm using the 1.0 range on the Bartington Instruments magnetic susceptibility meter (model MS2) with an 8-cm-diameter loop. The magnetic susceptibility provides another measure to assist cross-hole correlations and can help to detect fine variations in magnetic intensity associated with magnetic reversals. The quality of these results degrades in XCB and RCB sections where the core liner is not completely filled and/or the core is disturbed. However, the general downhole trends may still be used for stratigraphic correlation.

Thermal Conductivity

Whole-round core sections were allowed to adjust to room temperature for at least 4 hr before measuring thermal conductivities. The needle probe method was used in full-space configuration for soft sediments (Von Herzen and Maxwell, 1959), and in half-space mode for lithified sediment and hard rock samples (Vacquier, 1985). Thermal conductivities were typically measured in alternate sections. During transit to the first site and at irregular intervals during the cruise, the needle probes were calibrated vs. known standards (red rubber, black rubber, and macor), providing for five measurements in each standard per needle. A least-squares linear regression of known thermal conductivity and measured conductivity was performed for each needle to provide the corrections used for data reduction. Data are reported in units of (W/m·K), with an uncertainty of 5% to 10%, estimated from the regression line.

Soft Sediment "Full-Space" Measurements

Needle probes, containing a heater wire and a calibrated thermistor, were inserted into the sediment through small holes drilled into the core liners before the sections were split. The probes were positioned where the sample appeared to show uniform properties. Data were acquired using a Thermcon-85 unit interfaced to an IBM-PC compatible microcomputer. This system allowed up to five probes to be connected and operated simultaneously. For quality control, one probe was used with a standard of known conductivity during each run.

At the beginning of each measurement, temperatures in the samples were monitored without applying current to the heating element to verify that temperature drift was less than 0.04°C/min. The heater then was turned on and the temperature rise in the probes was recorded. After heating for about 60 s, the needle probe response behaves nearly as a line source with constant heat generation per unit length. Temperatures recorded between 60 and 240 s were fit to the following equation using the least-squares method (Von Herzen and Maxwell, 1959):

$$T(t) = (q/4\pi k)\ln(t) + L(t), \quad (2)$$

where k is the apparent thermal conductivity (W/m·K), T is temperature (°C), t is time (s), and q is the heat input per unit length of wire per unit time. The term $L(t)$ corrects for a linear change in temperature with time, described by the following equation:

$$L(t) = A \cdot t + T_e, \quad (3)$$

where A represents the rate of temperature change, and T_e is the equilibrium temperature. $L(t)$ therefore corrects for the background temperature drift, systematic instrumental errors, probe response, and sample geometry. The best fit to the data determines the unknown terms k and A.

Lithified Sediment and Hard Rock "Half-Space" Measurements

Half-space measurements were performed on selected lithified sediments and crystalline rock samples after the cores were split and the faces of the split cores were polished. The needle probe rested between the polished surface and a grooved epoxy block having relatively low conductivity (Sass et al., 1984; Vacquier, 1985). Half-space measurements were conducted in a water bath to keep the samples saturated, to improve the thermal contact between the needle and the sample, and to reduce thermal drift. EG&G thermal joint compound was used to improve the thermal contact. Data collection and reduction procedures for half-space tests are similar to those for full-space tests, except for a multiplicative constant in Equation 3 that accounts for the different experimental geometry.

Discrete Measurements

Index Properties

Index properties, including bulk density, grain density, water content, and porosity, were calculated from measurements of wet and dry sample masses and wet volumes. On samples of approximately 10 cm^3 dry sample volumes, which can be determined indirectly from the raw measurements listed above, also were measured directly, allowing one to check the calculations. In addition, bulk density was measured on unsplit cores using the GRAPE, as discussed above.

Sample mass was determined to a precision of ±0.01 g using a Scitech electronic balance. The sample mass was counterbalanced by a known mass such that the mass differentials generally were less than 1 g. Sample volumes were determined using a Quantachrome Penta-Pycnometer, a helium-displacement pycnometer with a nominal precision of ±0.02 cm^3, but a lower apparent experimental precision. Sample volumes were measured at least twice, and the mean of the readings was taken to be the volume. A reference volume was run with each group of samples, and rotated among the cells to check for systematic error. This exercise demonstrated that the measured volumes had a precision of about 0.03 cm^3. The pycnometer volumes were re-calibrated frequently during use for both small and large sample holders. The sample beakers used for discrete determinations of index properties were calibrated carefully prior to the cruise.

Water Content

There are two definitions for pore-water content: (1) W_d, pore-water mass divided by the mass of solids M_s, and (2) W_w, pore-water mass divided by total mass M_t. When determining water content, the methods of the American Society for Testing and Materials were followed (ASTM, designation [D] 2216; ASTM, 1989). The total (M_t) and dry (M_d) masses were measured using the electronic balance. The difference (M_t-M_d), after correction for salt by assuming a pore-water salinity (r) of 0.035, following the discussion by Boyce (1976), was taken as the pore-fluid mass. The equations for the two water-content calculations are as follows:

$$W_d \text{ (dry mass)} = (M_t - M_d) / (M_d - r \cdot M_t), \quad (4)$$

$$W_w \text{ (wet mass)} = (M_t - M_d) / (1 - r) M_t, \quad (5)$$

Bulk Density and Grain Density

Bulk density (ρ) is the density of the total sample including the pore fluid (i.e., $\rho = M_t/V_t$, where V_t is the total sample volume [cm^3] measured with the helium pycnometer).

Grain Density

Grain density, ρ_g is determined from the dry mass (Scitec balance) and dry volume (pycnometer) measurements. In this case, both mass and volume must be corrected for salinity, leading to the following equation:
is the density of salt (2.257 g/cm^3).

$$\rho_g = (M_d - M_s) / (V_d - [M_s / \rho_s]), \quad (6)$$

where V_d is the dry volume (cm^3) and ρ_s is the density of salt (2.257 g/cm^3). $M_s = r \cdot M_w$ is the mass of salt in the pore fluid, M_w is the mass of the seawater:

$$M_w = (M_t - M_d)/(1 - r). \quad (7)$$

To check these determinations, and to assess the quality of the volumes derived from the helium pycnometer, grain density was estimated occasionally using dry volume measurements in powdered samples.

Porosity

Porosity (η), the ratio of the fully saturated pore-water volume to the total volume, can be determined several ways using the quantities derived above. The following relationship using calculated grain density, ρ_g, and bulk density ρ was employed:

$$\eta = (\rho_g - \rho) / (\rho_g - \rho_w), \quad (8)$$

where ρ_g is grain density, ρ is bulk density and ρ_w is seawater density. To check for internal consistency, porosities also were calculated using the relationship:

$$\eta = (W_d \times \rho) / ([1 + W_d] \times \rho_w), \quad (9)$$

where ρ is bulk density and W_d is water content (dry mass).

Velocity Measurements

Discrete compressional-wave (P-wave) velocity measurements were obtained using two different systems, depending on the degree of lithification of the material. A Digital Sound Velocimeter (DSV) is a digital data acquisition system developed to measure and record compressional wave velocities and attenuation in soft sediments. The velocity calculation is based on the traveltime of an acoustic impulse between two piezoelectric transducers that are inserted directly into the split core. The transducers emit a 2-µs pulse having a repetition rate of 60 Hz. Gains from 0 to 42 dB can be applied to the received signal. The transmitted and received signals are displayed by a Nicolet 320 digital oscilloscope and transferred to a microcomputer for processing. The DSV software sums the waveforms from 3 to 10 successive digital records and displays the resulting waveform on the oscilloscope. Traveltime is estimated by visual identification of the first break on the stacked waveform and is corrected for the total delay caused by the transducers and other velocimeter hardware. Velocity is determined from the corrected traveltime and the measured distance (by caliper) between the transducers. The traveltime correction was determined by measuring the velocity of a distilled water sample and comparing the result to the standard water velocity (Wilson, 1960).

The Hamilton Frame Velocimeter (Hamilton, 1971) was used to measure compressional-wave velocities for well-indurated sediments, lithified sediments, and crystalline rocks. Velocity was determined using an impulsive signal having a frequency of 500 kHz. Cubes were trimmed from the sediment samples using a knife, with faces oriented parallel to the axis and split surface of the core. Velocity was measured in three mutually perpendicular directions, V (along the core axis), H_x (perpendicular to core axis and parallel to core face), and H_y (perpendicular to core face). The magnitude of acoustic anisotropy was estimated according to the relationship:

$$\text{Anisotropy} = 3(V_{max} - V_{min})/(V + H_x + H_y), \quad (10)$$

where V_{max} and V_{min} are the maximum and minimum velocities (among V, H_x, and H_y). In crystalline rocks minicore samples (2.54-cm diameter) were drilled perpendicular to the axis and face of the core. The ends of the minicores were trimmed parallel with a rock saw, and velocity (H_v) was measured along the axis of the minicore. Whenever possible, velocity measurements were made adjacent to paleomagnetic measurements, to allow the possibility of orientating the samples to geographic coordinates.

The dimensions of samples measured in the Hamilton Frame were determined with a digital linear caliper. Traveltime was estimated by visual identification of the first break of the stacked waveform, as described for the DSV measurements. Traveltime was corrected for the total delays caused by the transducers and velocimeter hardware. This was estimated by a linear regression of traveltime vs. distance for a series of aluminum and lucite standards. Velocities were calculated from the corrected traveltimes and measured sample dimensions. Velocity data are reported here in raw form; however, corrections to in-situ temperature and pressure also can be made using the relationships in Wyllie et al. (1956).

Electrical Resistivity

Resistivity was measured during Leg 149 using a four-probe configuration (Wenner spread) having two current and two potential electrodes. The electrodes, separated along the axis of the core, were pushed approximately 2 mm into and normal to the split core surface. The resistance of the saturated sediment was derived from the potential difference and instrument current using Ohm's law.

The resistivity data for the sediments are presented in terms of the formation factor (FF), which is the ratio of the resistivity of the saturated sediment to the resistivity of the pore fluid. The resistivity of the pore fluid was assumed to be the same as that of seawater (Boyce, 1980). The FF was calculated by dividing the resistance of the sample by the resistance of the seawater at room temperature, measured with the same apparatus. For consolidated sediments and hard rocks, electrical resistivity was measured in drilled minicores using an electrical resistivity cell.

Undrained Shear Strength

The undrained shear strength (S_u) of the sediment was determined using a Wyckham-Farrance motorized miniature vane shear device following the procedures of Boyce (1977). The vane rotation rate was set to 90°/min. Measurements were performed only in the fine-grained units having soft consistencies. The vane used for all measurements has a blade height of 1.27 cm and a diameter of 1.27 cm.

The instrument measures and records the torque and strain at the vane shaft using a torque transducer and potentiometer, respectively. The shear strength reported is the peak strength determined from the torque vs. strain plot. The residual strength is given by the steady-state strength of the material following failure (Pyle, 1984). It is assumed during this test that a cylinder of sediment shears uniformly about the axis of the vane in an undrained condition, and cohesion is the principal contributor to shear strength. However, progressive cracking within the sediment, pore pressure drainage, or local inhomogeneities can degrade the quality of the measurements.

DOWNHOLE LOGGING

Logging Tool Strings

Downhole logs are used to determine in-situ physical and chemical properties of formations adjacent to the borehole. Continuous, in-situ measurements provide stratigraphic, lithologic, geophysical, and mineralogic characterizations of a site. After coring is completed at a hole, a tool string (a combination of several sensors) is lowered down the hole on a conductor cable, and each sensor continuously monitors some property of the adjacent formation. Data typically are recorded at 15-cm intervals, though this figure depends on the sensor. The depths of investigation into the formation are also sensor-dependent.

Three Schlumberger logging tool strings were used during Leg 149 (Fig. 12): the geophysical combination (Quad-combo), the geochemical combination (GLT), and the Formation MicroScanner (FMS) combination. The Lamont-Doherty Earth Observatory (LDEO) temperature tool (TLT) was attached to the base of all tool strings to obtain downhole formation/fluid temperatures. The natural gamma-ray tool (NGT) was run as part of each tool string to correlate depths between logging runs.

The geophysical tool string used during Leg 149 (Fig. 12A) consisted of the dipole shear imager (DSI) for measuring sonic velocities; the high-temperature lithodensity tool (HLDT) for measuring formation bulk density and photoelectric effect (PEF); the phasor induction tool (DIT) for measuring electrical resistivity; and the natural

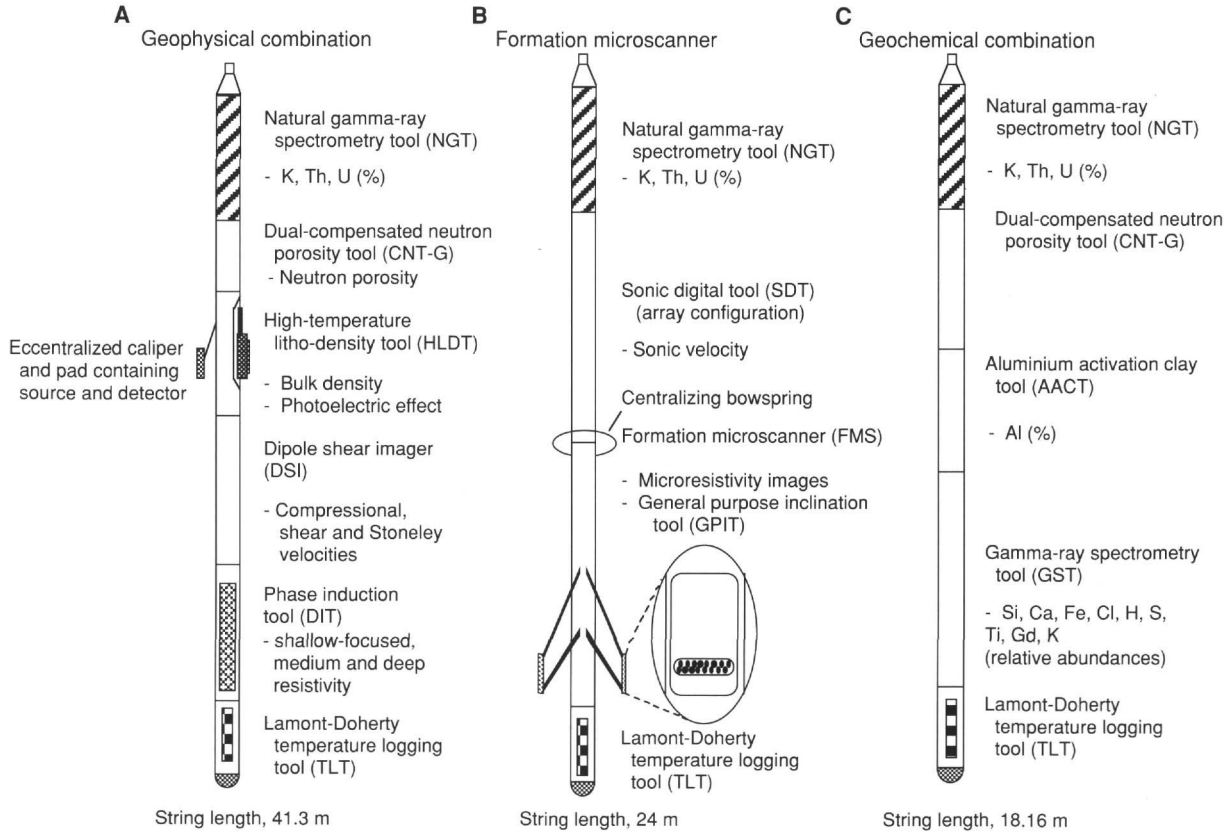

Figure 12. Diagram showing the logging tool strings deployed during Leg 149.

gamma-ray tool (NGT) for measuring the natural radioactivity of the formation and for correlating between logging runs. A caliper on the HLDT indicated hole diameter.

The geochemical combination used during Leg 149 (Fig. 12C) consisted of the NGT tool, the aluminum clay tool (ACT), and the gamma-ray spectrometry tool (GST). This tool combination measures the relative concentrations of Si, Ca, Al, Fe, S, H, Cl, K, U, and Th.

The FMS tool string used during Leg 149 (Fig. 12B) consisted of an array sonic tool (SDT) and the FMS tool, which was coupled to a general purpose inclinometer tool (GPIT). The FMS and GPIT provided a spatially oriented microresistivity image of the borehole wall, as well as a caliper measurement. The SDT provided an alternative measurement of sonic velocities for comparison with the DSI tool.

For Leg 149, Schlumberger deployed their new Maxis 500 digital logging unit in conjunction with the "old" Offshore Service Unit (OSU). The "new" Maxis 500 system was capable, during Leg 149, of processing data from only the geophysical and FMS tool strings; the GLT was operated by the OSU unit. Data from the Maxis 500 was generated in a new data format (digital log information standard [DLIS]). For Leg 149, this was converted to log information standard (LIS) format for compatibility with shipboard and shore-based logging software.

Logging Tools

A brief description of logging tools run during Leg 149 is given in the following sections. A detailed description of logging tool principles and applications is provided in Ellis (1987), Schlumberger (1989), Serra (1984), and Timur and Toksöz (1985). The specifics of each tool are summarized in Table 7, and the approximate vertical resolutions of the tools are given in Table 8. The HLDT, DIT, NGT, ACT, GST, FMS, and GPIT tools are described in the "Explanatory Notes" chapter of the Leg 144 *Initial Reports* volume Shipboard Scientific Party, 1993b). The sonic tools, DSI and SDT, and the temperature tool, TLT, are described below.

Sonic Tools

Sonic tools measure compressional-wave traveltimes between a transmitter and receiver. This provides a direct measure of vertical traveltime in the adjacent formation (the interval traveltime [delta T]), which is used to calculate the porosity of the formation and sonic velocity. The product of velocity and density logs is an impedance log. A synthetic seismogram may be produced from the impedance log for comparison with seismic reflection profiles across the site.

Sonic Digital Tool or the "Array Sonic Configuration" (SDT-C)

The SDT-C sonic tool maximizes the information obtained by digitizing the complete seismic waveform. The tool has two transmitters and receivers with a 1-m spacing in addition to a linear array of eight receivers spaced at 15 cm, with a transmitter-receiver distance starting at 3.33 m (see Fig. 13A). The addition of a linear array in place of two discrete receivers is the main change from the earlier SDT tool. The digitally recorded full waveform is used later to deter-

Table 7. Summary of logging tools and their application for Leg 149.

Tool	Acronym	Principle	Usable through pipe	Combinable (1)	Synthetic seismogram (2)	Lithology mineralogy (3)	Porosity	Geochemistry elements	Notes	Used during Leg 149	Typical data available on board ship
Sonic	LSS/SDT BHC	Traveltime of sound (2 receivers)	No	1	G	F	G			No	
Sonic	SDT-C/DSST	Traveltime of sound (8-10 receivers)	No		VG	F	G		(6)	Yes	Velocity
Resistivity											
Shallow	SFL	Focused current	No	1	F	F	VG			Yes	Resistivity
Medium	ILM	Induced current	No	1	F	F	VG			Yes	Resistivity
Deep	ILD	Induced current	No	1	F	F	VG			Yes	Resistivity
Gamma ray	GR	Natural gamma-ray emissions	No	1	P	VG				Yes	Gamma-ray counts
Caliper	MCD	Hole diameter	No	1		P			(4)	No	
Dual laterolog	DLL	Resistivity to current	No		F	F	VG			No	
Neutron porosity	CNTG	Absorption of bombarding neutrons	Yes	1/2	P	F	VG	H		Yes	Porosity
Spectral gamma-ray	NGT	Natural gamma-ray emissions	Yes	1/2/3/4	P	VG		K, Th, U		Yes	K, Th, U abundances
Bulk density	HLDT	Absorption of bombarding gamma rays	No	1/2/3	G	G	G			Yes	Density
Induced gamma-ray spectroscopy	GST	Capture of bombarding neutrons	Yes	3	F	VG	F	Ca, Si, Fe,S,Ti, Gd, H, Cl		Yes	Relative elemental yields
Aluminum clay tool	ACT	Absorption of bombarding neutrons	Yes	3	P	F	P	Al, Mn		Yes	Aluminum abundance
Formation microscanner	FMS	Focused microcurrent	No	4	P	P	G		(5)	Yes	Resitivity images, 2-axis caliper
12-Channel sonic	MCS	Traveltime of sound (12 receivers)	No		VG	F	G		(6)	No	
Borehole televiewer	BHTV	Traveltime + reflectivity of borehole wall	No		P	F			(7)	No	
3-Axis magnetometer	GPIT	Oriented magnetic field including inclination	No	1/2/3/4	P	F			(8)	Yes	Hole dip, inclination
Temperature	TLT	Formation temperature	Yes	1/2/3/4						Yes	Temperature

Notes: Usefulness of tool for application: VG = very good; G = good; F= fair; P = poor. (1) Tools having the same number may be combined in a string. (2) Logs other than sonic and density can be converted to pseudosonic/density, based on known log responses to lithology and porosity. (3) Percentages of minerals with abundance > 3% were determined from simultaneous inversion of several logs. (4) Quality control for other logs. (5) Detailed mapping of fractures, faults, foliations, and formation structures; analysis of depositional environments; formation dip. (6) Shear velocity, apparent attenuation. (7) Stress directions, fracture orientation, structural dip, formation morphology. (8) Magnetic reversals, stratigraphy, fault zones.

mine shear-wave and Stoneley-wave velocities in addition to the compressional velocity obtained immediately. The tools standard vertical resolution is 60 cm, although special array processing can improve resolution to 15 cm.

Dipole Shear Imager (DSI)

The DSI consists of one dual-frequency (14 and 1 kHz) monopole transmitter and two pairs of dipole transmitters (2.2 kHz). The dipole transmitters create a "uni-directional" flexing of the borehole wall that excites shear waves, in contrast to more common "omnidirectional" monopole sources. The receiver consists of an array of eight receiver groups with a 15-cm spacing. Within each receiver group, four receivers are in line with the dipole transmitters (Fig. 13B). Like the SDT described above, the DSI can measure compressional- and Stoneley-wave velocities, but has the added advantage that it can measure shear-wave velocity directly in "soft" formations (where the shear-wave velocity is less than the velocity of the drilling fluid, such as a poorly lithified sediment). Besides the conventional first-motion detection methods, DSI uses digital correlation analysis between signals from the receiver array to determine wave propagation velocities. Full waveforms are digitally recorded to allow post-cruise extraction of additional information, such as seismic attenuation. The ratio of compressional- to shear-wave velocities provides information about porosity and lithology. Observation of the reflection, attenuation, and dispersion of Stoneley waves provide useful information about permeability and fracture aperture identification in the immediate vicinity of the borehole.

Table 8. Approximate vertical resolution of various logging tools used during Leg 149.

Tool	Vertical resolution	Depth of investigation
Phasor induction tool (DIT)		
ILD Deep resistivity	200, 88, 59 cm	1.5 m
ILM Medium resistivity	150, 88, 59 cm	76 cm
SFL Shallow focused	59 cm	38 cm
Natural gamma-ray tool (NGT)	46 cm 15–30 cm	Variable
Lithodensity tool (HLDT)		Variable
Density, photoelectric effect	49 cm (6 in. sampling) 35 cm (2 in. sampling) 20 cm Alpha processing 30 cm Alpha processing (2 in. sampling)	15–60 cm
Dipole shear imager (DSI)	30 cm Special processing 15 cm	Variable 10–60 cm
Sonic digital tool (SDT-C/array)	30 cm Special processing 15 cm	Variable 10–60 cm
Gamma-ray spectroscopy tool (GST)	15 cm	30 cm 12–20 cm
Aluminum activation tool (AACT)	25 cm 12–20 cm	Variable
Dual porosity compensated neutron tool (CNT-G)	55 cm (6 in. sampling) 33 cm Alpha proc. (6 in. sampling) 25.4 cm Alpha proc. (2 in. sampling)	Variable and porosity (15–60 cm)
Formation microscanner (FMS)	6 mm	5–25 cm
Lamont temperature tool (TLT)	(A) 1 fast-response (1-s time constant reading/s; (B) slow-response, high-accuracy reading (10-s time constant)/10-s; *vertical resolution depends on logging speed.*	

Note: Standard sampling is at 15 cm (6 in.) intervals. High resolution sampling is at 5.5 cm (2 in.) intervals. ALPHA is a special high resolution processing routine. Depth of investigation is formation and environment specific; these depths are only rough estimates/ranges.

Lamont Temperature Tool (TLT)

The TLT is a self-contained temperature recording tool that can be attached to any Schlumberger tool string. Data from two thermistors and a pressure transducer are collected at a pre-determined rate of one sample per 0.5 to 5.0 s and stored within the tool. Following the logging run, data are transferred from the tool to a shipboard computer for analysis. A fast-response, lower accuracy, thermistor is able to detect sudden temperature excursions such as might be caused by fluid flow from the formation. A slow-response, higher accuracy, thermistor can be used to estimate borehole fluid temperature. If the history of drilling-fluid circulation in the hole and at least two temperature logs are available (Jaeger, 1961), one can estimate the post-drilling equilibrium geotherm. Conversion to depth is based on pressure recordings from the pressure transducer and on correlation with winch time "wire-out" records. During Leg 149, to save time in downloading, we used two temperature tools alternately, one tool (used on the geophysical and geochemical strings) had both fast-and slow-response thermistors, while the second contained only a slow-response thermistor. New Macintosh-based software was implemented for processing the temperature data.

Quality of Log Data

The quality of log data may be seriously degraded by rapid changes in the diameter of a hole and in sections where the borehole diameter is greatly increased or has been washed out. The result of these effects is to impair logging by causing "bridging" or "tool sticking"

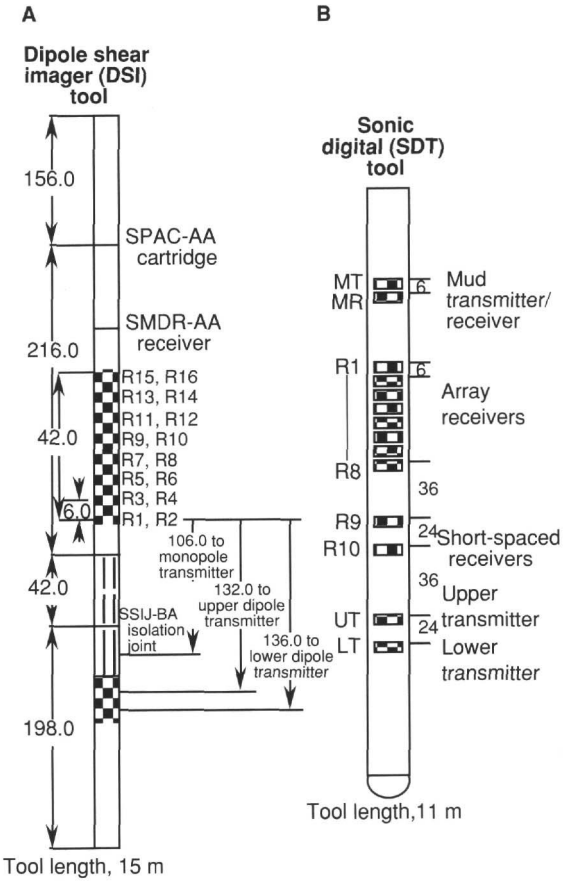

Figure 13. Diagram showing the two sonic tools deployed during Leg 149. The spacings of components are given in inches.

and to increase the volume of fluid between the formation and the logging tool. Deep investigation devices, such as resistivity and velocity tools, are least sensitive to borehole effect. Nuclear measurements (density, neutron porosity, and both natural and induced spectral gamma-rays) are more sensitive because of their shallower depth of investigation and because of the effect of increased volume of drilling fluid on attenuation of neutrons and gamma rays. Corrections can be applied to the original data to reduce these effects. However, one cannot correct for very large washouts.

By using the NGT on each string, data can be depth-correlated between logging runs. Logs from different tool strings, however, may still have minor depth mismatches caused by either cable stretching or ship's heave during recording. Small errors in depth-matching can impair the multilog analyses in zones of rapidly varying lithology. Ship's heave is minimized by a hydraulic wireline heave compensator designed to adjust for ship motion during logging operations. Precise depth-matching of logs to cores is difficult in zones where core recovery is low because of the inherent ambiguity of placing the recovered section within the cored interval.

Analysis of Logs

During each logging run, incoming data were observed in real time on a monitor in the Maxis logging unit and simultaneously were recorded on disk. After logging, data were processed and reformatted with the Terralog log-interpretation software package. FMS data were processed on board the ship using Schlumberger "Logos" software. Preliminary log interpretation was conducted aboard the ship. Further FMS and geochemical log processing and the final depth-shifting and data quality control were undertaken after the leg at the Borehole Research Laboratory of LDEO.

CD-ROM Materials

Structure

The CD-ROM in the back of this volume is a "data only" CD-ROM that contains both depth-shifted and processed logging data that has been provided by the Borehole Research Group at Lamont-Doherty Earth Observatory, as well as shipboard Gamma-Ray Attenuation Porosity Evaluation (GRAPE), index properties, and magnetic susceptibility data of cores collected on board *JOIDES Resolution* during Legs 149, 150, and 150X (land-based portion of Leg 150). Also included on this CD-ROM is the Macintosh image viewing application NIH image. CD-ROM production was done by the Borehole Research Group at Lamont-Doherty Earth Observatory, wireline logging operator for ODP.

The INDEX file contains a summary of all the files loaded on the CD-ROM. The software documentation file in the GENERAL INFORMATION directory contains information on which software packages work best to import portable bit map (PBM-8-bit binary) raster files. It also includes network sources for the graphics software and data compression information. The README file gives information about whom to contact with any questions about the production of or data on the CD-ROM.

All of the ASCII files (basic logging and dipmeter files) are TAB delimited for compatibility with most spreadsheet and data base programs. Holes that have long logging runs are often divided into TOP, MIDDLE, and BOTTOM directories. Were the data collected continuously or were two or more sections of data spliced together, the files would be in the SPLICED directory.

In the FMS-PBM format subdirectory are two subdirectories: 1:1 ratio with maximum 10-m-long image raster files and 1:10 ratio with maximum 100-m-long image raster files. The image raster files are named according to their depth interval. The raster documentation files contain image file parameter information necessary for use with most graphic software packages.

IN-SITU TEMPERATURE MEASUREMENTS

Water-sampling Temperature Probe (WSTP) Temperature Measurements

The WSTP tool is described in the Leg 141 *Initial Reports* volume, "Explanatory Notes" chapter (Shipboard Scientific Party, 1992).

The WSTP was inserted and left in place for at least 15 min during each deployment. If taken, fluid samples were not drawn until the probe had been in place for 15 min because the influx of fluids might bias the temperature measurements.

APC Tool (ADARA) Temperature Measurements

The ADARA tool is described in the Leg 141 *Initial Reports* volume, "Explanatory Notes" chapter (Shipboard Scientific Party, 1992). During Leg 149, the ADARA tool collected temperature measurements at 5-s intervals over a 15-min period.

Data Reduction

The data reduction method for both the WSTP and ADARA temperature probes estimates the steady-state, bottom-hole temperature by forward modeling the recorded transient temperature curve as a function of time. The shape of the transient temperature curve is determined by the response function of the tool and the thermal properties of the bottom-hole sediments (Bullard, 1954; Horai and Von Herzen, 1985). In general, temperature increases following emplacement of the probe are caused by frictional heating of the probe tip during insertion. The temperature peaks after a short period of time and decreases monotonically thereafter, approaching the steady-state temperature of the sediments at a rate inversely proportional to time. Data reduction software developed by Andy Fisher and Moses Sun for WSTP data and provided with the ADARA tool for those data were used during Leg 149 to model interactively the transient temperature curve and to extrapolate for the equilibrium temperature. Variables in the modeling method are the thermal conductivity of the sediments, tool insertion time, delay time between tool insertion and peak temperature, and the length of the portion of the curve to be fit. In practice, relatively few iterations of the modeling procedure were required to obtain reasonable fits to the temperature data that were consistent with the thermal conductivity measurements obtained as part of the routine analysis of physical properties. For all temperature extrapolations, we used 1.3 W/(m·K) for thermal conductivity of the sediment around the probe.

Several potential sources of error contribute to limiting the accuracy of the equilibrium temperature estimated from the WSTP data. First, heating of the probe on insertion is not instantaneous, as the processing software assumes. Because the time of insertion is not known with great precision, some uncertainty is unavoidable in the duration of the transient thermal signal. In practice, this problem was resolved by applying an empirical time shift to the thermal data in such a way as to best fit the theoretical transient response functions of Bullard (1954). Second, the probe was not always completely inserted, may have been inserted into cuttings in the bottom of the borehole, or may have fractured the bottom-hole sediments upon insertion. In these instances, one is usually unable to recover reliable steady-state temperatures. However, one is able to recognize the presence of such problems by the shape of the temperature-time curve, thus avoiding the use of faulty data. The combined effects of

these uncertainties can lead to an estimated accuracy of ± 0.1 °C in the unreduced temperature measurements.

Temperature differences within a tool run are more precise than the absolute temperatures, therefore we shifted temperatures from multiple runs to match the seafloor temperatures. Further, we used the data only to compute temperature gradient and heat flow results. These do not depend on absolute temperatures.

Temperature gradient was determined at each site to be the slope of a best fitting line to the temperature as a function of depth.

Heat flow is the slope of the best fitting line to temperature as a function of vertically integrated thermal resistivity (VITR). Thermal resistivity is the reciprocal of thermal conductivity. VITR is the integral, from the seafloor to a given depth, of the thermal resistivity. VITR for each site was calculated by a numerical integration of the reciprocal of measured thermal conductivity. In a medium having vertically varying thermal conductivity and only vertical conductive heat transport, temperature is a linear function of VITR.

REFERENCES*

ASTM, 1989. *Annual Book of ASTM Standards for Soil and Rock; Building Stones: Geotextiles* (Vol. 04.08): Philadelphia (Am. Soc. Testing Materials).

Behrmann, J.H., Lewis, S.D., Musgrave, R.J., et al., 1992. *Proc. ODP, Init. Repts.,* 141: College Station, TX (Ocean Drilling Program).

Berggren, W.A., Kent, D.V., and Flynn, J.J., 1985. Jurassic to Paleogene: Part 2. Paleogene geochronology and chronostratigraphy. *In* Snelling, N.J. (Ed.), *The Chronology of the Geological Record.* Geol. Soc. London Mem., 10:141-195.

Berggren, W.A., Kent, D.V., Flynn, J.J., and Van Couvering, J.A., 1985. Cenozoic geochronology. *Geol. Soc. Am. Bull.,* 96:1407-1418.

Berggren, W.A., Kent, D.V., and Van Couvering, J.A., 1985. The Neogene: Part 2. Neogene geochronology and chronostratigraphy. *In* Snelling, NJ. (Ed.), *The Chronology of the Geological Record.* Geol. Soc. London Mem., 10:211-260.

Blatt, H., Middleton, G.V., and Murray, R., 1980. *Origin of Sedimentary Rocks* (2nd ed.): Englewood Cliffs, NJ (Prentice-Hall).

Blow, W.H., 1969. Late middle Eocene to Recent planktonic foraminiferal biostratigraphy. *In* Brönniman, P., and Renz, H.H. (Eds.), *Proc. First Int. Conf. Planktonic Microfossils, Geneva, 1967:* Leiden (E.J. Brill), 1:199-422.

Bolli, H.M., and Saunders, J.B., 1985. Oligocene to Holocene low latitude planktonic foraminifera. *In* Bolli, H.M., Saunders, J.B., and Perch-Nielsen, K. (Eds.), *Plankton Stratigraphy:* Cambridge (Cambridge Univ. Press), 155-262.

Boyce, R.E., 1976. Definitions and laboratory techniques of compressional sound velocity parameters and wet-water content, wet-bulk density, and porosity parameters by gravimetric and gamma ray attenuation techniques. *In* Schlanger, S.O., Jackson, E.D., et al., *Init. Repts. DSDP,* 33: Washington (U.S. Govt. Printing Office), 931-958.

——, 1977. Deep Sea Drilling Project procedures for shear strength measurement of clayey sediment using modified Wykelam Farrance Laboratory Vane apparatus. *In* Barker, P.P., Dalziel, I.W.D., et al., *Init. Repts. DSDP,* 36: Washington (U.S. Govt. Printing Office), 1059-1068.

——, 1980. Determination of the relationships of electrical resistivity, sound velocity, and density/porosity of sediment and rock by laboratory techniques and well logs from Deep Sea Drilling Project Sites 415 and 416 off the coast of Morocco. *In* Lancelot, Y., Winterer, E.L., et al., *Init. Repts. DSDP,* 50: Washington (U.S. Govt. Printing Office), 305-318.

Bralower, T.J., and Siesser, W.G., 1992. Cretaceous calcareous nannofossil biostratigraphy of Sites 761, 762, and 763, Exmouth and Wombat Plateaus, northwest Australia. *In* von Rad, U., Haq, B.U., et al., *Proc. ODP, Sci. Results,* 122: College Station, TX (Ocean Drilling Program), 529-556.

Bukry, D., 1973. Low-latitude coccolith biostratigraphic zonation. *In* Edgar, N.T., Saunders, J.B, et al., *Init. Repts. DSDP,* 15: Washington (U.S. Govt. Printing Office), 685-703.

——, 1975. Coccolith and silicoflagellate stratigraphy, northwestern Pacific Ocean, Deep Sea Drilling Project Leg 32. *In* Larson, R.L., Moberly, R., et al., *Init. Repts. DSDP,* 32: Washington (U.S. Govt. Printing Office), 677-701.

Bullard, E.G., 1954. The flow of heat through the floor of the Atlantic Ocean. *Proc. R. Soc. London A,* 222:408-29.

Cande, S.C., and Kent, D.V., 1992. A new geomagnetic polarity time scale for the Late Cretaceous and Cenozoic. *J. Geophys. Res.,* 97:13917-13951.

Collot, J.-Y, Greene, H.G., Stokking, L.B., et al., 1992. *Proc. ODP, Init. Repts.,* 134: College Station, TX (Ocean Drilling Program).

Dick, H.J.B., Erzinger, J., Stokking, L.B., et al., 1992. *Proc. ODP, Init. Repts.,* 140: College Station, TX (Ocean Drilling Program).

Ellis, D.V., 1987. *Well Logging For Earth Scientists:* New York (Elsevier).

Engleman, E.E., Jackson, L.L., and Norton, D.R., 1985. Determination of carbonate carbon in geological materials by coulometric titration. *Chem. Geol.,* 53:125-128.

Espitalié, J., 1980. Role of mineral matrix in kerogen pyrolysis: influence on petroleum generation and migration. *AAPG Bull.,* 64:59-66.

Espitalié, J., Deroo, G., and Marquis, F, 1986. La pyrolyse Rock-Eval et ses applications. *Rev. Inst. Fr. Pet.,* 41:73-89.

Evans, H.B., and Cotterell, C.H., 1970. Gamma-ray attenuation density scanner. *In* Peterson, M.N.A., et al., *Init. Repts. DSDP,* 2: Washington (U.S. Govt. Printing Office), 460-472.

Gartner, S., 1977. Calcareous nannofossil biostratigraphy and revised zonation of the Pleistocene. *Mar. Micropaleontol.,* 2:1-25.

——, 1990. Neogene calcareous nannofossil biostratigraphy, Leg 116 (Central Indian Ocean). *In* Cochran, J.R., Stow, D.A.V., et al., *Proc. ODP, Sci. Results,* 116: College Station, TX (Ocean Drilling Program), 165-187.

Gieskes, J.M., and Peretsman, G., 1986. Water chemistry procedures aboard *JOIDES Resolution*—some comments. *ODP Tech. Note, 5.*

Hallam, A., Hancock, J.M., LaBrecque, J.L., Lowrie, W., and Channell, J.E.T., 1985. Jurassic to Paleogene: Part 1. Jurassic and Cretaceous geochronology and Jurassic to Paleogene magnetostratigraphy. *In* Snelling, NJ. (Ed.), *The Chronology of the Geological Record.* Geol. Soc. London Mem., 10:118-140.

Hamilton, E.L., 1971. Prediction of in-situ acoustic and elastic properties of marine sediments. *Geophysics,* 36:266-284.

Harland, W.B., Armstrong, R.L., Cox, A.V, Craig, L.E., Smith, A.G., and Smith, D.G., 1990. *A Geologic Time Scale 1989:* Cambridge (Cambridge Univ. Press), 263.

Horai, K., and Von Herzen, R.P., 1985. Measurement of heat flow on Leg 86 of the Deep Sea Drilling Project. *In* Heath, G.R., Burckle, L.H., et al., *Init. Repts. DSDP,* 86: Washington (U.S. Govt. Printing Office), 759-777.

Jaeger, J.C., 1961. The effect of the drilling fluid on temperatures measured in boreholes. *J. Geophys. Res.,* 66:563-569.

Katz, B.J., 1983. Limitations of "Rock-Eval" pyrolysis for typing organic matter. *Org. Geochem.,* 4:195-199.

Kennett, J.P., and Srinivasan, M.S., 1983. *Neogene Planktonic Foraminifera: A Phylogenetic Atlas:* Stroudsburg, PA (Hutchinson Ross).

Kvenvolden, K.A., and McDonald, T.J., 1986. Organic geochemistry on the *JOIDES Resolution—an* assay. *ODP Tech. Note,* 6.

Lundberg, N., and Moore, J.C., 1986. Macroscopic structural features in Deep Sea Drilling Project cores from forearc regions. *In* Moore, J.C. (Ed.), *Structural Fabrics Preserved in Deep Sea Drilling Project Cores From Forearcs.* Mem.—Geol. Soc. Am., 166:13-44.

Martini, E., 1971. Standard Tertiary and Quaternary calcareous nannoplankton zonation. *In* Farinacci, A. (Ed.), *Proc. 2nd Int. Conf. Planktonic Microfossils Roma:* Rome (Ed. Tecnosci.), 2:739-785.

Mazzullo, J.M., Meyer, A., and Kidd, R., 1987. New sediment classification scheme for the Ocean Drilling Program. *In* Mazzullo, J., and Graham, A.G. (Eds.), *Handbook for Shipboard Sedimentologists.* ODP Tech. Note, 8:45-67.

Munsell Soil Color Charts, 1971. Baltimore, MD (Munsell Color).

Norrish, K., and Hutton, J.T., 1969. An accurate X-ray spectrographic method for the analysis of a wide range of geological samples. *Geochim. Cosmochim. Acta,* 33:431-453.

* Abbreviations for names of organizations and publication titles in ODP reference lists follow the style given in *Chemical Abstracts Service Source Index* (published by American Chemical Society).

Okada, H., and Bukry, D., 1980. Supplementary modification and introduction of code numbers to the low-latitude coccolith biostratigraphic zonation (Bukry, 1973; 1975). *Mar. Micropaleontol.,* 5:321-325.

Perch-Nielsen, K., 1979. Calcareous nannofossils from the Cretaceous between the North Sea and the Mediterranean. *In* Wiedmann, J. (Ed.), *Aspekte der Kreide Europas.* Int. Union Geol. Sci. Ser. A, 6:223-272.

——, 1985. Mesozoic calcareous nannofossils. *In* Bolli, H.M., Saunders, J.B., and Perch-Nielsen, K. (Eds.), *Plankton Stratigraphy:* Cambridge (Cambridge Univ. Press), 329-426.

Peters, K.E., 1986. Guidelines for evaluating petroleum source rock using programmed pyrolysis. *AAPG Bull.,* 70:318-329.

Pyle, M.R., 1984. Vane shear data on undrained residual strength. *J. Geotech. Engr. Div., Am. Sac. Civ. Eng.,* 110:543-547.

Reynolds, R.C., Jr., 1967. Matrix corrections in trace element analysis by X-ray fluorescence: estimation of the mass absorption coefficient by Compton scattering. *Am. Mineral.,* 48:1133-1143.

Rio, D., Raffi, I., and Villa, G., 1990. Pliocene-Pleistocene calcareous nannofossil distribution patterns in the Western Mediterranean. *In* Kastens, K.A., Mascle, J., et al., *Proc. ODP, Sci. Results,* 107: College Station, TX (Ocean Drilling Program), 513-533.

Roth, P.H., 1978. Cretaceous nannoplankton biostratigraphy and oceanography of the northwestern Atlantic Ocean. *In* Benson, W.E., Sheridan, R.E., et al., *Init. Repts. DSDP,* 44: Washington (U.S. Govt. Printing Office), 731-760.

Sass, J.H., Kennelly, J.P., Jr., Smith, E.P., and Wendt, W.E., 1984. Laboratory line-source methods for the measurement of thermal conductivity of rocks near room temperature. *U.S. Geol. Surv. Tech. Rep.*

Schlumberger, 1989. *Log Interpretation Principles/Applications:* Houston, TX (Schlumberger Educational Services).

Serra, O., 1984. *Fundamentals of Well Log Interpretation* (Vol. 1): *The Acquisition of Logging Data:* Amsterdam (Elsevier).

Shepard, F., 1954. Nomenclature based on sand-silt-clay ratios. *J. Sediment. Petrol.,* 24:151-158.

Shipboard Scientific Party, 1990. Explanatory notes. *In* Rangin, C., Silver, E.A., von Breymann, M.T., et al., *Proc. ODP, Init. Repts.,* 124: College Station, TX (Ocean Drilling Program), 7-33.

——, 1992. Explanatory notes. *In* Behrmann, J.H., Lewis, S.D., Musgrave, R.J., et al., *Proc. ODP, Init. Repts.,* 141: College Station, TX (Ocean Drilling Program), 37-71.

——, 1993a. Explanatory notes. *In* Gillis, K., Mével, C., Allan, J., et al., *Proc. ODP, Init. Repts.,* 147: College Station, TX (Ocean Drilling Program), 15-42.

——, 1993b. Explanatory notes. *In* Premoli Silva, I., Haggerty, J., Rack, F., et al., *Proc. ODP, Init. Repts.,* 144: College Station, TX (Ocean Drilling Program), 15-42.

——, 1993c. Explanatory notes. *In* Rea, D.K., Basov, I.A., Janecek, TR., Palmer-Julson, A., et al., *Proc. ODP, Init. Repts.,* 145: College Station, TX (Ocean Drilling Program), 9-33.

Sigal, J., 1977. Essai de zonation du Crétacé méditerranéen à l'aide des foraminifères planctoniques. *Geol. Mediterr.,* 4:99-108.

Sissingh, W., 1977. Biostratigraphy of Cretaceous nannoplankton. *Geol. Mijnbouw,* 56:37-50.

Taira, A., Hill, I., Firth, J.V., et al., 1991. *Proc. ODP, Init. Repts.,* 131: College Station, TX (Ocean Drilling Program).

Timur, A., and Toksöz, M.N., 1985. Fundamentals of well log interpretation. *Annu. Rev. Earth Planet. Sci.,* 13:315-344.

Toumarkine, M., and Luterbacher, H., 1985. Paleocene and Eocene planktic foraminifera. *In* Bolli, H.M., Saunders, J.B., and Perch-Nielsen, K. (Eds.), *Plankton Stratigraphy:* Cambridge (Cambridge Univ. Press), 87-154.

Vacquier, V, 1985. The measurement of thermal conductivity of solids with a transient linear heat source on the plane surface of a poorly conducting body. *Earth Planet. Sci. Lett.,* 74:275-279.

van Morkhoven, F.P.C.M., Berggren, W.A., and Edwards, A.S., 1986. Cenozoic cosmopolitan deep-water benthic foraminifera. *Bull. Cent. Rech. Explor.-Prod. Elf-Aquitaine,* Mem. 11.

Von Herzen, R.P., and Maxwell, A.E., 1959. The measurement of thermal conductivity of deep-sea sediments by a needle-probe method. *J. Geophys. Res.,* 64:1557-1563.

Wentworth, C.K., 1922. A scale of grade and class terms of clastic sediments. *J. Geol.,* 30:377-392.

Wilson, W.D., 1960. Speed of sound in seawater as a function of temperature, pressure and salinity. *J. Acoust. Soc. Am.,* 32:641-644.

Wyllie, M.R.J., Gregory, A.R., and Gardner, L.W., 1956. Elastic wave velocities in heterogeneous and porous media. *Geophysics,* 21:41-70.

Ms 149IR-102